

# Error Rates for Kernel Classification under Source and Capacity Conditions

Hugo Cui<sup>1</sup> Bruno Loureiro<sup>2</sup> Florent Krzakala<sup>2</sup> Lenka Zdeborová<sup>1</sup>

## Abstract

In this manuscript, we consider the problem of kernel classification under the Gaussian data design, and under source and capacity assumptions on the dataset. While the decay rates of the prediction error have been extensively studied under much more generic assumptions for kernel ridge regression, deriving decay rates for the classification problem has been hitherto considered a much more challenging task. In this work we leverage recent analytical results for learning curves of linear classification with generic loss function to derive the rates of decay of the misclassification (prediction) error with the sample complexity for two standard classification settings, namely margin-maximizing Support Vector Machines (SVM) and ridge classification. Using numerical and analytical arguments, we derive the error rates as a function of the source and capacity coefficients, and contrast the two methods.

## 1. Introduction

Kernel methods (Nadaraja, 1964; Watson, 1964) are still today widely used techniques in the machine learning toolbox, and are also studied as a limiting case for more complex neural networks (Neal, 1996; Williams, 1996; Jacot et al., 2018; Lee et al., 2018; Chizat et al., 2019). Kernels allow to leverage the expressivity of non-linear features, while still remaining rephrasable in terms of a linear parametric (and hence relatively simpler to analyze) learning problem in the feature space associated to the kernel. In this dual picture, the complexity of the learning task, as captured by its generalization error, is often characterized by the relative decay of the spectrum of the features covariance (*the capacity*) and that of the coefficients of the target function expressed in the feature basis (*the source*). The error rates for the kernel

regression problem using ridge loss have been extensively and rigorously characterized in the seminal work of (Caponnetto & Vito, 2005; Caponnetto & De Vito, 2007), and a sizeable body of work in the statistical learning (Steinwart et al., 2009; Lin et al., 2018; Jun et al., 2019; Liu et al., 2020) as well as in statistical physics (Sollich & Halees, 2002; Spigler et al., 2020; Bordelon et al., 2020; Cui et al., 2021) has been devoted thereto. On the other hand, deriving explicit error rates for kernel *classification* tasks has been hitherto considered a more challenging, and hence lesser understood, problem.

**Main contribution** — In this work, we investigate the decay rate of the misclassification (generalization) error for kernel classification, under the Gaussian design and source/capacity regularity assumptions with capacity coefficient  $\alpha$  and source coefficient  $r$ . Building on the analytic framework of (Loureiro et al., 2021), we consider the two most widely used classifiers: margin-maximizing Support Vector Machines (SVMs) and ridge classifiers. Combining analytical and numerical arguments, we show in Section 3 that the error rate (describing the decay of the prediction error with the number of samples) for margin-maximizing SVM is

$$\epsilon_g^{\text{SVM}} \sim n^{-\frac{\alpha \min(r, \frac{1}{2})}{1 + \alpha \min(r, \frac{1}{2})}},$$

which we contrast with the rate for ridge classification, which we establish in Section 4 to be

$$\epsilon_g^{\text{ridge}} \sim n^{-\frac{\alpha \min(r, 1)}{1 + 2\alpha \min(r, 1)}}$$

when optimally regularized. We argue in the light of these findings that the SVM always displays faster rates than the ridge classifier for the classification task considered. In addition, we observe that some real datasets fall under the considered setting, and illustrate in Section 5 how their learning curves are to a good degree described by the aforementioned rates.

**Related work** — The analysis of kernel ridge regression is a classical topic (Caponnetto & Vito, 2005; Caponnetto & De Vito, 2007; Steinwart et al., 2009; Fischer & Steinwart, 2020; Lin et al., 2018; Bartlett et al., 2020; Lin et al., 2018; Jun et al., 2019; Lin et al., 2018; Cui et al., 2021). In particular, generalization error rates have been studied

<sup>1</sup>École Polytechnique Fédérale de Lausanne (EPFL), Statistical Physics of Computation lab, CH-1015 Lausanne <sup>2</sup>École Polytechnique Fédérale de Lausanne (EPFL), Information Learning and Physics lab, CH-1015 Lausanne. Correspondence to: Hugo Cui <hugo.cui@epfl.ch>.

both in the noisy (Caponnetto & Vito, 2005; Caponnetto & De Vito, 2007) and noiseless (Spigler et al., 2020; Bordelon et al., 2020) settings, and some of these rates were furthermore shown to be achievable by stochastic gradient descent (Pillaud-Vivien et al., 2018; Berthier et al., 2020; Varre et al., 2021).

Source and capacity conditions are regularity assumptions that are standard in the study of kernel features, see e.g. (Marteau-Ferey et al., 2019; Pillaud-Vivien et al., 2018). They allow to subsume a large class of learning setups in terms of two numbers, the *source* and *capacity* coefficients, which characterize the complexity of the learning task in feature space. The Gaussian design assumption has also been widely employed, notably to study kernel ridge regression (Dobriban & Wager, 2018; Dicker et al., 2016; Hsu et al., 2012). The work of (Cui et al., 2021) has shown that, for the kernel ridge regression task, the error rates derived under the Gaussian design hypothesis were identical to those proven in more generic worst-case analyses (Lin et al., 2018; Jun et al., 2019; Caponnetto & Vito, 2005; Caponnetto & De Vito, 2007; Bartlett et al., 2020).

The study of error rates for SVMs (Vapnik et al., 1996; Drucker et al., 1996; Cortes & Vapnik, 2004) is still a relatively uncharted research topic, with the exception of some specific cases, e.g. for polynomial target functions (Dietrich et al., 1999b; Oppel & Urbanczik, 2001) or for the Parzen estimate (Krzyżak, 1986). Decay rates for the *loss function*, but not the prediction error, have on the other hand been characterized by (Marteau-Ferey et al., 2019).

## 2. Setting

### 2.1. Kernel classification

Consider a dataset  $\mathcal{D} = \{(x^\mu, y^\mu)\}_{\mu=1}^n$  with  $n$  independent samples from a probability measure  $\nu$  on  $\mathcal{X} \times \{-1, +1\}$ , with  $\mathcal{X} \subset \mathbb{R}^d$ . We will assume that the labels can be expressed as

$$y^\mu = \text{sign}(f^*(x^\mu)) \quad (1)$$

for some target function  $f^* : \mathcal{X} \rightarrow \mathbb{R}$ . Learning to classify  $\mathcal{D}$  in the direct space  $\mathcal{X}$  for a *linear*  $f^*$  has been the object of extensive studies. In the present work, we focus on the case where  $f^*$  more generically belongs to the space of square-integrable functions  $L^2(\mathcal{X})$ . To classify  $\mathcal{D}$ , a natural method is then to perform *kernel classification* in a  $p$ -dimensional Reproducing Kernel Hilbert Space (RKHS)  $\mathcal{H}$  associated to a kernel  $K$ , by minimizing the regularized empirical risk:

$$\hat{\mathcal{R}}_n(f) = \frac{1}{n} \sum_{\mu=1}^n \ell(f(x^\mu), y^\mu) + \lambda \|f\|_{\mathcal{H}}^2. \quad (2)$$

The function  $\ell(\cdot)$  is a loss function and  $\lambda$  is the strength of the  $\ell_2$  regularization term. In this paper we shall more

specifically consider the losses  $\ell(z, y) = \max(0, 1 - yz)$  (hinge classification) and  $\ell(z, y) = (y - z)^2$  (ridge classification), and the case of an infinite dimensional RKHS ( $p = \infty$ ). The risk (2) admits a dual rewriting in terms of a standard parametric risk. To see this, diagonalize  $K$  in an orthogonal basis of *kernel features*  $\{\psi_k(\cdot)\}_{k=1}^p$  of  $L^2(\mathcal{X})$ , with corresponding eigenvalues  $\{\omega_k\}_{k=1}^p$ :

$$\int_{\mathcal{X}} \nu(dx') K(x, x') \psi_k(x') = \omega_k \psi_k(x). \quad (3)$$

It is convenient to normalize the eigenfunctions to

$$\int_{\mathcal{X}} \nu(dx) \psi_k(x)^2 = \omega_k, \quad (4)$$

so that the kernel  $K$  can be rewritten in simple scalar product form  $K(x, x') = \psi(x)^\top \psi(x')$ , where we named  $\psi(x)$  the  $p$ -dimensional vector with components  $\{\psi_k(x)\}_{k=1}^p$ . Furthermore, note that the covariance  $\Sigma$  of the data in feature space with this choice of feature map is simply diagonal

$$\Sigma = \mathbb{E}_{x \sim \nu}(\psi(x) \psi(x)^\top) = \text{diag}(\omega_1, \dots, \omega_p). \quad (5)$$

Any function  $f \in \mathcal{H}$  can then be expressed as  $f(\cdot) = w^\top \psi(\cdot)$  for a vector  $w$  with square summable components. Using this parametrization, the risk (2) can be rewritten as

$$\hat{\mathcal{R}}_n(w) = \frac{1}{n} \sum_{\mu=1}^n \ell(w^\top \psi(x^\mu), y^\mu) + \lambda w^\top w. \quad (6)$$

Throughout this manuscript we will refer to the components of the target function in the features basis as the *teacher*  $\theta^*$ , so that

$$f^*(\cdot) = \theta^{*\top} \psi(\cdot).$$

Similarly, the minimizer  $\hat{w}$  of the parametric risk (6) is related to the argmin  $\hat{f}$  of (2) by  $\hat{f}(\cdot) = \hat{w}^\top \psi(\cdot)$ , and will be referred to as the *estimator* in the following. We make two further assumptions: First, we work under the *Gaussian data design*, and assume the features  $\psi(x)$  to follow a Gaussian distribution with covariance  $\Sigma$ , i.e.  $\psi(x) \sim \mathcal{N}(0, \Sigma)$ . Even though this assumption might appear constraining, rates derived under Gaussian design can hold more broadly. For instance, the rates established by (Cui et al., 2021) under Gaussian design were later proven by (Jin et al., 2021) under weaker conditions on the features. We will moreover discuss in Section 5 several settings in which our theoretical rates are in good agreement with rates observed for real data.

Second, following (Cui et al., 2021), we assume that the *regularization strength*  $\lambda$  decays as a *power-law* of the number of samples  $n$  with an exponent  $\ell$ :  $\lambda = n^{-\ell}$ . Note that this form of regularization is natural, since the need for regularizing is lesser for larger training sets. Furthermore, this allows to investigate the classical question of the *asymptotically*

optimal regularization (Caponnetto & Vito, 2005; Caponnetto & De Vito, 2007; Cui et al., 2021), i.e. the decay  $\ell$  of the regularization yielding fastest decrease of the prediction error.

## 2.2. Source and capacity conditions

Under the above assumptions of Gaussian data design with data covariance  $\Sigma$  and existence of a teacher  $\theta^*$  that generates the labels using eq. (1) we can now study the error rates. In statistical learning theory one often uses the *source and capacity conditions*, which assume the existence of two parameters  $\alpha > 1, r \geq 0$  (hereafter referred to as the *capacity coefficient* and the *source coefficient* respectively) so that

$$\text{tr} \Sigma^{\frac{1}{\alpha}} < \infty, \quad \theta^{*\top} \Sigma^{1-2r} \theta^* < \infty. \quad (7)$$

As in (Dobriban & Wager, 2018; Spigler et al., 2020; Bordelon et al., 2020; Berthier et al., 2020; Cui et al., 2021), we will consider the particular case where both the spectrum of  $\Sigma$  and the teacher components  $\theta_k^*$  have exactly a power-law form satisfying the limiting source/capacity conditions (7):

$$\omega_k = k^{-\alpha}, \quad \theta_k^* = k^{-\frac{1+\alpha(2r-1)}{2}}. \quad (8)$$

The power-law forms (8) have been empirically found in (Cui et al., 2021) in the context of kernel regression to be a reasonable approximation for some simple real datasets including MNIST and Fashion MNIST and some standard kernels such as polynomial kernels and radial basis functions. Similar observations were also made in the present work and are discussed in Appendix. E and section 5.

The capacity parameter  $\alpha$  and source parameter  $r$  capture the complexity of the dataset. A large  $\alpha$ , for example, signals that the spectrum of the data covariance  $\Sigma$  displays a fast decay, implying that the data effectively lies along a small number of directions, and has a low effective dimension. Conversely, a small capacity  $\alpha$  means that the data is effectively large dimensional, and therefore a priori harder to learn. Similarly, a large  $r$  signals a good alignment of the teacher  $\theta^*$  with the main directions of the data, and a priori an easier learning task. In terms of the target function  $f^*$ , larger  $r$  correspond to smoother  $f^*$ . Note that  $r \geq \frac{1}{2}$  implies that  $f^* \in \mathcal{H}$ , while  $r \leq \frac{1}{2}$  implies  $f^* \in L^2(\mathcal{X}) \setminus \mathcal{H}$ .

Finally, note that while (Marteau-Ferey et al., 2019) suggested an alternative definition for the source and capacity coefficients in the case of non-square loss functions, their redefinition is not directly applicable for the hinge loss.

## 2.3. Misclassification error

The performance of learning the dataset  $\mathcal{D}$  using kernel classification (6) is quantified by the misclassification (generalization) error

$$\epsilon_g = \frac{1}{2} - \frac{1}{2} \mathbb{E}_{\mathcal{D}} \mathbb{E}_{x,y \sim \nu} (y \text{sign}(\hat{w}^\top \psi(x))), \quad (9)$$

where  $\hat{w}$  is the minimizer of the risk (6). The error (9) corresponds to the probability for the predicted label  $\text{sign}(\hat{w}^\top \psi(x))$  of a test sample  $x$  to be incorrect. The rate at which the error (9) decays with the number of samples  $n$  in  $\mathcal{D}$  depends on the complexity of the dataset, as captured by the source and capacity coefficients  $\alpha, r$  eq. (8). To compute this rate, we build upon the work of (Loureiro et al., 2021) who, following a long body of work in the statistical physics literature (Mézard et al., 1987; Dietrich et al., 1999a; Engel & Van den Broeck, 2001; Mézard & Montanari, 2009; Bordelon et al., 2020; Advani et al., 2020), provided and proved a mathematically rigorous closed form asymptotic characterization of the misclassification error as

$$\epsilon_g = \frac{1}{\pi} \arccos(\sqrt{\eta}), \quad \eta = \frac{m^2}{\rho q}, \quad (10)$$

where  $\rho$  is the squared  $L^2(\mathcal{X})$  norm of the target function  $f^*$ , i.e.

$$\rho = \int_{\mathcal{X}} \nu(dx) f^*(x)^2 = \theta^{*\top} \Sigma \theta^*, \quad (11)$$

and  $m, q$  are the solution of a set of self-consistent equations, which are later detailed and analyzed in section 3 for margin-maximizing SVMs and section 4 for ridge classifiers. The order parameters  $m, q$  are known as the *magnetization* and the *self-overlap* in statistical physics and respectively correspond to the target/estimator and estimator/estimator  $L^2(\mathcal{X})$  correlations:

$$m = \mathbb{E}_{\mathcal{D}} \int_{\mathcal{X}} \nu(dx) f^*(x) \hat{f}(x) = \mathbb{E}_{\mathcal{D}} (\hat{w}^\top \Sigma \theta^*),$$

$$q = \mathbb{E}_{\mathcal{D}} \int_{\mathcal{X}} \nu(dx) \hat{f}(x)^2 = \mathbb{E}_{\mathcal{D}} (\hat{w}^\top \Sigma \hat{w}). \quad (12)$$

It follows from these interpretations that  $\eta$  has to be thought of as the *cosine-similarity* between the teacher  $\theta^*$  and the estimator  $\hat{w}$ , with perfect alignment ( $\eta = 1$ ) resulting in minimal error  $\epsilon_g = 0$  from (9).

Note that while this characterization has formally been proven in (Loureiro et al., 2021) in the asymptotic proportional  $n, p \rightarrow \infty, n/p = \mathcal{O}(1)$  limit, we are presently using it in the  $n \ll p = \infty$  limit, thereby effectively working at  $n/p = 0^+$ . The non-asymptotic rate guarantees of (Loureiro et al., 2021) are nevertheless encouraging in this respect, although a finer control of the limit would be warranted to put the present analysis on fully rigorous grounds. Further, (Cui et al., 2021) also build on (Loureiro et al., 2021) in the  $n/p = 0^+$  limit, and display reassuring numerics-backed results, later rigorously proven by (Jin et al., 2021). We thus conjecture that this limit can be taken as well safely in our case.

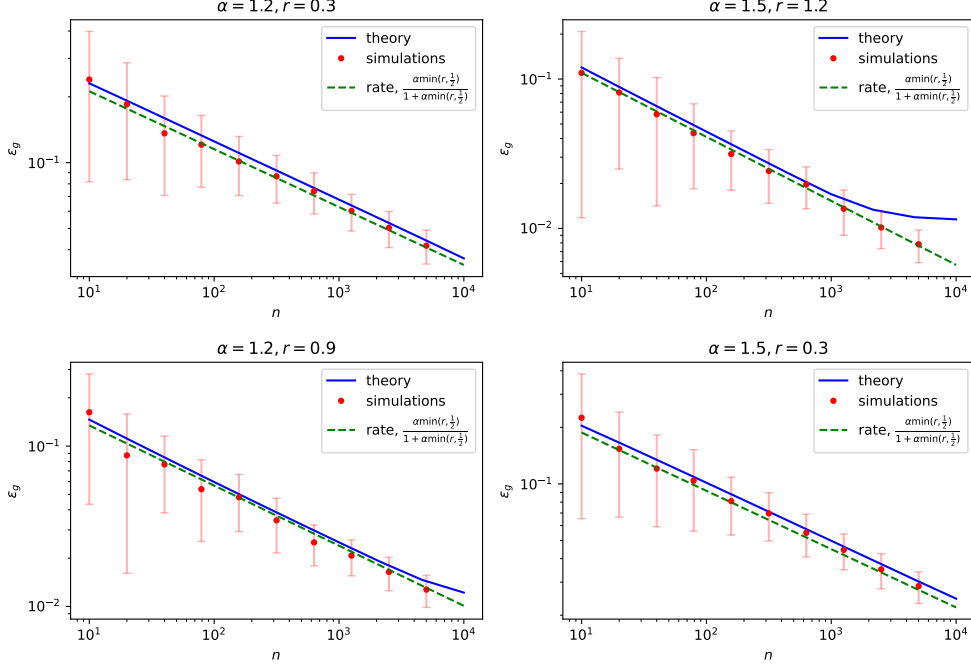


Figure 1. Misclassification error  $\epsilon_g$  for max-margin classification on synthetic Gaussian data, as specified in (8), for different source/capacity coefficients  $\alpha, r$ . In blue, the solution of the closed set of equations (14) used in the characterization (9) for the misclassification error, using the `g3m` package (Loureiro et al., 2021). The dimension  $p$  was cut-off at  $10^4$ . Red dots corresponds to simulations using the `scikit-learn` SVC package run for vanishing regularization  $\lambda = 10^{-4}$  and averaged over 40 instances, for  $p = 10^4$ . The green dashed line indicates the power-law rate (16) derived in this work.

### 3. Max-margin classification

#### 3.1. Self-consistent equations

In this section we study regression using Support Vector Machines. The risk (6) then reads for the hinge loss

$$\hat{\mathcal{R}}_n(w) = \frac{1}{n} \sum_{\mu=1}^n \max(0, 1 - y^\mu w^\top \psi(x^\mu)) + \lambda w^\top w. \quad (13)$$

In the following, we shall focus more specifically on the max-margin limit with  $\lambda = 0^+$ . We argue in Appendix B that zero regularization is indeed asymptotically optimal for the data following eq. (8) when the target function is characterized by a source  $r \leq \frac{1}{2}$ , i.e.  $f^* \in L^2(\mathcal{X}) \setminus \mathcal{H}$ . We heuristically expect margin maximization to be *a fortiori* optimal also for easier and smoother teachers  $f^* \in \mathcal{H}$ . For the risk (13) at  $\lambda = 0^+$ , the self-consistent equations defining  $m, q$  in (12) read (see Appendix A)

$$\begin{cases} \rho = \sum_{k=1}^{\infty} \theta_k^{*2} \omega_k, \\ m = \hat{r}_1 \frac{n}{z} \sum_{k=1}^{\infty} \frac{\omega_k^2 \theta_k^{*2}}{1 + \frac{n}{z} \omega_k}, \\ q = \hat{r}_1^2 \frac{n^2}{z^2} \sum_{k=1}^{\infty} \frac{\theta_k^{*2} \omega_k^3}{(1 + \frac{n}{z} \omega_k)^2} + \hat{r}_2 \frac{n}{z^2} \sum_{k=1}^{\infty} \frac{\omega_k^2}{(1 + \frac{n}{z} \omega_k)^2} \end{cases},$$

$$\begin{cases} \hat{r}_1 = \frac{1}{2\pi\sqrt{\rho}} \left( \frac{\sqrt{2\pi}(1 + \text{erf}(\frac{1}{\sqrt{2q(1-\eta)}})) + 2e^{-\frac{1}{2q(1-\eta)}} \sqrt{q(1-\eta)}}{\int_{-\infty}^{\frac{1}{\sqrt{q}}} dx \frac{e^{-\frac{1}{2}x^2}}{\sqrt{2\pi}} [1 + \text{erf}(\sqrt{\frac{\eta}{2(1-\eta)}} x)]} \right), \\ \hat{r}_2 = \frac{\frac{1}{\sqrt{q}} \int_{-\infty}^{\frac{1}{\sqrt{q}}} dx \frac{e^{-\frac{1}{2}x^2}}{\sqrt{2\pi}} [1 + \text{erf}(\sqrt{\frac{\eta}{2(1-\eta)}} x)] (1 - \sqrt{q}x)^2}{\left( \int_{-\infty}^{\frac{1}{\sqrt{q}}} dx \frac{e^{-\frac{1}{2}x^2}}{\sqrt{2\pi}} [1 + \text{erf}(\sqrt{\frac{\eta}{2(1-\eta)}} x)] \right)^2}, \\ z = \frac{\frac{1}{\sqrt{q}} \int_{-\infty}^{\frac{1}{\sqrt{q}}} dx \frac{e^{-\frac{1}{2}x^2}}{\sqrt{2\pi}} [1 + \text{erf}(\sqrt{\frac{\eta}{2(1-\eta)}} x)]}{\frac{z}{n} \sum_{k=1}^{\infty} \frac{\omega_k}{z + \omega_k}}. \end{cases} \quad (14)$$

Here  $\hat{r}_1$  should be thought of as the ratio between the norms of the estimator  $\hat{w}$  and the teacher  $\theta^*$ , while  $z$  can be loosely interpreted as an effective regularization. A detailed derivation of these equations can be found in Appendix A.

#### 3.2. Decay rates for max-margin

From the analytical and numerical investigation of the equations (14), as detailed in Appendix A, the following scalings are found to hold between the order parameters:

$$m \sim \sqrt{q} \sim \hat{r}_1 \sim n \left( \frac{z}{n} \right)^{\frac{1}{\alpha}} \sim n^{\frac{\alpha \text{amin}(r, \frac{1}{2})}{1 + \alpha \text{amin}(r, \frac{1}{2})}}. \quad (15)$$

Note that the mutual scaling between  $m$ ,  $q$ ,  $\hat{r}_1$  also follows intuitively from the interpretation of these order parameters, as provided in the discussion around eqs. (12) and (14). Since the width of the margin is generically expected to shrink with the number of samples (as more training data are likely to be sampled close to the separating hyperplane), the increase of the norm of  $\hat{w}$  (as captured by  $q, \hat{r}_1$ ) with  $n$  is also intuitive. Finally, an analysis of the subleading corrections to  $m$  and  $q$ , detailed in Appendix A, leads to

$$\epsilon_g \sim n^{-\frac{\alpha \min(r, \frac{1}{2})}{1 + \alpha \min(r, \frac{1}{2})}}. \quad (16)$$

The error rate (16) stands in very good agreement with numerical simulations on artificial Gaussian datasets generated using the model specification (8), see Fig. 1.

Two observations can further be made on the decay rate (16). First, the rate is as expected an increasing function of  $\alpha$  (low-dimensionality of the features) and  $r$  (smoothness of the target  $f^*$ ). Second, for a source  $r \geq \frac{1}{2}$  (corresponding to a target  $f^* \in \mathcal{H}$ ), the rate saturates, suggesting that all functions in  $\mathcal{H}$  are all equally easy to classify, while for rougher target  $f^* \in L^2(\mathcal{X}) \setminus \mathcal{H}$  the specific roughness of the target function, as captured by its source coefficient  $r$ , matters and conditions the rate of decay of the error.

## 4. Ridge classification

### 4.1. Self-consistent equations

Another standard classification method is the ridge classifier, which corresponds to minimizing the risk

$$\hat{\mathcal{R}}_n(w) = \frac{1}{n} \sum_{\mu=1}^n (y^\mu - w^\top \psi(x^\mu))^2 + \lambda w^\top w. \quad (17)$$

As previously discussed in section 2, we consider a decaying regularization  $\lambda = n^{-\ell}$ . The self-consistent equations characterizing the quantities  $(q, m)$ , read for the ridge risk (17)

$$\begin{cases} \rho = \sum_{k=1}^{\infty} \theta_k^{*2} \omega_k, \\ m = \sqrt{\frac{2}{\pi \rho}} \frac{n}{z} \sum_{k=1}^{\infty} \frac{\omega_k^2 \theta_k^{*2}}{1 + \frac{n}{z} \omega_k}, \\ q = \frac{n^2}{z^2} \sum_{k=1}^{\infty} \frac{\frac{2}{\pi \rho} \theta_k^{*2} \omega_k^3 + \frac{1+q-2m\sqrt{\frac{2}{\pi \rho}}}{n} \omega_k^2}{\left(1 + \frac{n}{z} \omega_k\right)^2}, \\ z = n\lambda + \frac{z}{n} \sum_{k=1}^{\infty} \frac{\lambda_k}{\lambda_k + \frac{z}{n}}. \end{cases} \quad (18)$$

Further details on the derivation of (18) from (Loureiro et al., 2021) are provided in Appendix C. Like (14), eqs. (18) have been formally proven in the proportional  $n, p \rightarrow \infty$ ,  $n/p = \mathcal{O}(1)$  limit in (Loureiro et al., 2021), but are expected to hold also in the present  $n \ll p = \infty$  setting

(Cui et al., 2021; Jin et al., 2021). Note that comparing to (14), eqs. (18) correspond to a constant student/teacher norm ratio  $\hat{r}_1$  and to a simple  $\hat{r}_2$ :

$$\hat{r}_1 = \frac{2}{\pi \rho}, \quad \hat{r}_2 = 1 + q - 2m\sqrt{\frac{2}{\pi \rho}}. \quad (19)$$

$\hat{r}_2$  moreover admits a very intuitive interpretation as the prediction mean squared error (MSE) between the true label  $y = \text{sign}(\theta^{*\top} \psi(x))$  and the pre-activation linear predictor  $\hat{w}^\top \psi(x)$ , i.e.

$$\hat{r}_2 = \mathbb{E}_{\psi(x)} \left( \text{sign} \left( \theta^{*\top} \psi(x) \right) - \hat{w}^\top \psi(x) \right)^2. \quad (20)$$

### 4.2. Decay rates for ridge classification

Similarly to (Bordelon et al., 2020; Cui et al., 2021), an analysis of the equations (18) (see Appendix C) reveals that, depending on how the rate of decay  $\ell$  of the regularization compares to the capacity  $\alpha$ , two regimes (called *effectively regularized* and *effectively un-regularized* in (Cui et al., 2021) in the context of ridge regression) can be found:

**Effectively regularized regime** –  $\ell < \alpha$ . In this regime, an analysis of the corrections to the self-overlap  $q$  and magnetization  $m$ , presented in Appendix C, shows that the misclassification error scales like

$$\epsilon_g \sim n^{-\frac{1}{2} \min(2\ell \min(r, 1), \frac{\alpha - \ell}{\alpha})}. \quad (21)$$

The rate (21) compares very well to numerical simulations, see Fig. 2. Note that the saturation for ridge happens for  $r = 1$ , rather than  $r = \frac{1}{2}$  as for max-margin classification (see discussion in section 3): very smooth targets  $f^*$  characterized by a source  $r \geq 1$  are all equally easily classified by ridge. For rougher teachers  $f^*$  characterized by  $r \leq 1$  however, the rate of decay of the error (21) depends on the specific roughness of the target, even if, in contrast to max-margin, the latter belongs to  $\mathcal{H}$  ( $r \geq \frac{1}{2}$ ). Two important observations should further be made on the rates (21):

- If the regularization remains small (fast decay  $\alpha > \ell > \alpha/(1 + 2\alpha \min(r, 1))$ ), the decay (21) is determined only by the data capacity  $\alpha$ , while the source  $r$  plays no role. As a matter of fact, with insufficient regularization, the limiting factor to the learning is the tendency to overfit, which depends on the effective dimension of the data as captured by the capacity  $\alpha$ .
- For larger regularizations (slow decays  $\ell < \alpha/(1 + 2\alpha \min(r, 1))$ ), the limiting factor becomes the complexity of the teacher  $\theta^*$ , as captured by the source  $r$ .

**Effectively un-regularized regime** –  $\ell > \alpha$ . As derived in Appendix C, the error plateaus and stays of order 1:

$$\epsilon_g = \mathcal{O}(1). \quad (22)$$



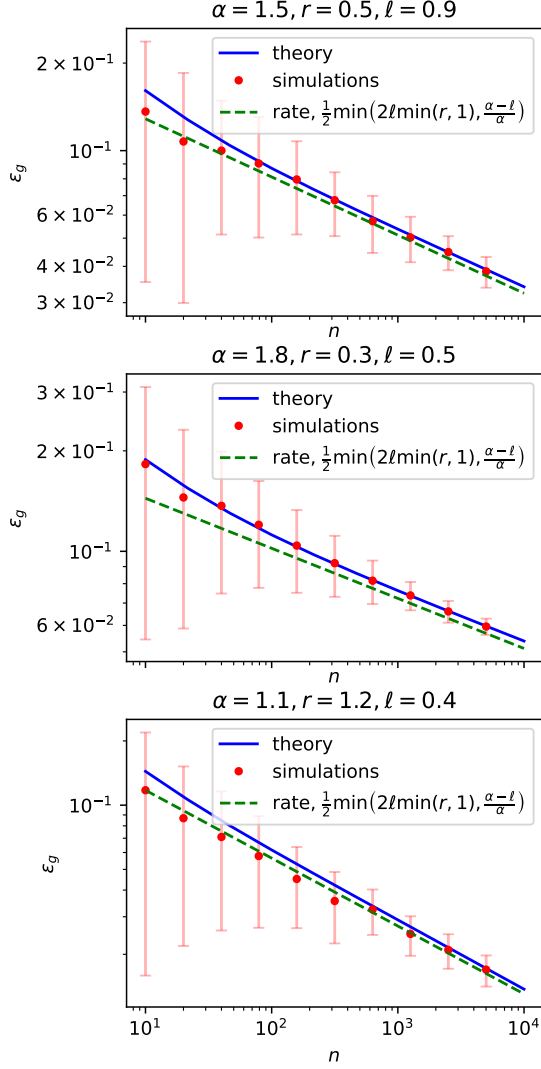


Figure 2. Misclassification error  $\epsilon_g$  for ridge classification on synthetic Gaussian data, as specified in (8), for different source/capacity coefficients  $\alpha, r$ , in the effectively regularized regime  $\ell < \alpha$ . In blue, the solution of the equations (14) used in the characterization (9) for the misclassification error, using the `g3m` package (Loureiro et al., 2021). The dimension  $p$  was cut-off at  $10^4$ . Red dots corresponds to simulations averaged over 40 instances, for  $p = 10^4$ . The green dashed line indicates the power-law (21) derived in this work.

This plateau is further elaborated upon in Appendix D, and is visible in numerical experiments, see Fig. 3. It corresponds to the first plateau in a double descent curve, with the second descent never happening since  $p = \infty$ . Intuitively, this phenomenon is attributable to the ridge classifier overfitting the labels using the small-variance directions of the data (8).

Interestingly, all the rates (22) and (21) correspond exactly (up to a factor  $\frac{1}{2}$ ) to those reported in (Cui et al., 2021) for

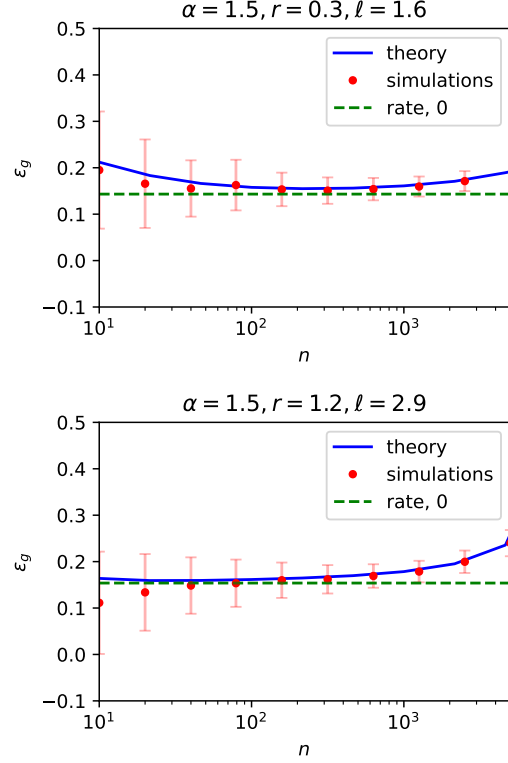


Figure 3. Misclassification error  $\epsilon_g$  for ridge classification on synthetic Gaussian data, as specified in (8), for different source/capacity coefficients  $\alpha, r$ , in the effectively non-regularized regime  $\ell > \alpha$ . In blue, the solution of the equations (14) used in the characterization (9) for the misclassification error, using the `g3m` package (Loureiro et al., 2021). The dimension  $p$  was cut-off at  $10^4$ . Red dots corresponds to simulations averaged over 40 instances, for  $p = 10^4$ . The green dashed line indicates the power-law (22) derived in this work. The slight increase of the error for larger  $n$  is due to finite size effects of the simulations ran at  $p = 10^4 < \infty$ . Physically, it corresponds to onset of the ascent preceding the second descent that is present for finite  $p$ , see Appendix D for further discussion.

the MSE of ridge regression, where they are respectively called the *red*, *blue* and *orange* exponents. Notably, the plateau (22) at low regularizations and the  $(\alpha - \ell)/\alpha$  exponent in (21) only appeared in (Cui et al., 2021) for noisy cases in which the labels are corrupted by an additive noise. The fact that they hold in the present *noiseless* study very temptingly suggests that model mis-specification (trying to interpolate binary labels using a linear model) effectively plays the role of a large noise.

### 4.3. Optimal rates

**Optimally regularized ridge classification** In practice, the strength of the regularization  $\lambda$  is a tunable parameter. A natural question to ask is then the one of the *asymptotically*

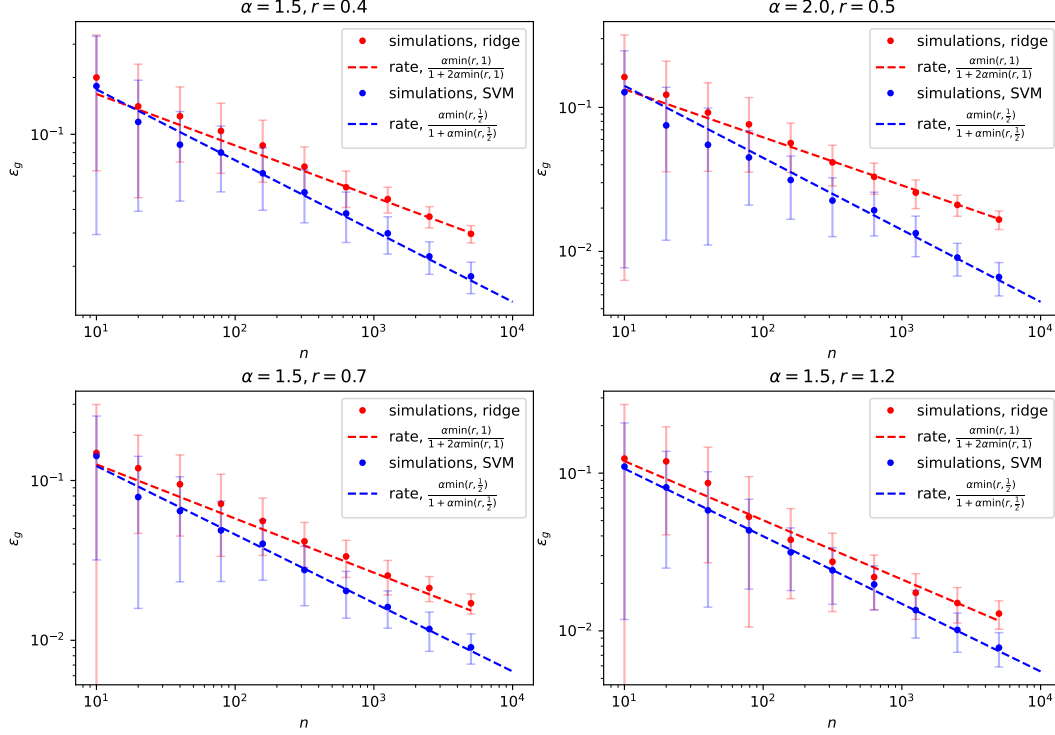


Figure 4. (red) Misclassification error  $\epsilon_g$  for ridge classification on synthetic Gaussian data, as specified in (8), for different source/capacity coefficients  $\alpha, r$ , for optimal regularization  $\lambda^*$ . The dimension  $p$  was cut-off at  $10^4$  and the regularization  $\lambda$  numerically tuned to minimize the error  $\epsilon_g$  for every  $n$ . Red dots corresponds to simulations averaged over 40 instances, for  $p = 10^4$ . Optimization over  $\lambda$  was performed using cross validation, with the help of the python `scikit-learn` `GridSearchCV` package. The red dashed line represents the power-law (24). In blue, the learning curves for max-margin for the same dataset are plotted for reference, along the corresponding power law (16).

optimal regularization, that is the regularization decay rate  $\ell^*$  leading to fastest decay rates for the misclassification error. From the expressions of (21) (which hold provided  $\ell < \alpha$ ) and (22) (which holds provided  $\ell > \alpha$ ), the value of  $\ell$  maximizing the error rate is found to be

$$\ell^* = \frac{\alpha}{1 + 2\alpha \min(r, 1)}, \quad (23)$$

and the corresponding error rate for  $\epsilon_g^* = \epsilon_g(\lambda^* = n^{-\ell^*})$  is

$$\epsilon_g^* \sim n^{-\frac{\alpha \min(r, 1)}{1 + 2\alpha \min(r, 1)}}, \quad (24)$$

see the green dashed lines in Fig. 4. Coincidentally, the optimal rate (24) is up to a factor  $\frac{1}{2}$  identical to the classical optimal rate known for the rather distinct problem of the MSE of kernel ridge regression on noisy data (Caponnetto & Vito, 2005; Caponnetto & De Vito, 2007). Like the max-margin exponent (16), the optimal error rate for ridge (24) is an increasing function of both the capacity  $\alpha$  and the source  $r$ , i.e. of the easiness of the learning task. Note that in contrast to max-margin classification which is insensitive to the specifics of the target function  $f^*$ , provided it is in  $\mathcal{H}$ ,

ridge is sensitive to the source (smoothness)  $r$  of  $f^*$  up to  $r = 1$ .

**Comparison to max-margin** A comparison of the max-margin rate  $a_{\text{SVM}} = \alpha \min(r, \frac{1}{2}) / (1 + \alpha \min(r, \frac{1}{2}))$  (16) and the optimal ridge exponent  $a_r = \alpha \min(r, 1) / (1 + 2\alpha \min(r, 1))$  (24) reveals that for any  $\alpha > 1, r \geq 0$ ,

$$a_{\text{SVM}} - a_r = \frac{a_{\text{SVM}} a_r}{\alpha} \left( \alpha + \frac{1}{\min(r, 1)} - \frac{1}{\min(r, \frac{1}{2})} \right) > 0. \quad (25)$$

In other words, the margin-maximizing SVM always displays faster rates than the ridge classifier for the class of data studied (8), see Fig. 4.

We finally briefly comment on support vector proliferation. (Muthukumar et al., 2021; Hsu et al., 2020; Ardeshir et al., 2021) showed that in some settings almost every training sample in  $\mathcal{D}$  becomes a support vector for the SVM. In such settings, the estimators  $\hat{w}$  (and hence the error  $\epsilon_g$ ) consequently coincide for the ridge classifier and the margin-maximizing SVM. In the present setting however, eq. (25) establishes that for features with a power-law decaying spec-

trum (8), there is *no* such support vector proliferation. Note that this result does not follow immediately from Theorem 3 in (Ardehshir et al., 2021). In fact, the spiked covariance (8), with only a small number of important (large variance) directions and a tail of unimportant (low-variance) directions does effectively not offer enough overparametrization (Bartlett et al., 2020; Hsu et al., 2020) for support vector proliferation, and the support consists only of the subset of the training set with weakest alignment with the spike.

## 5. Remarks for real datasets

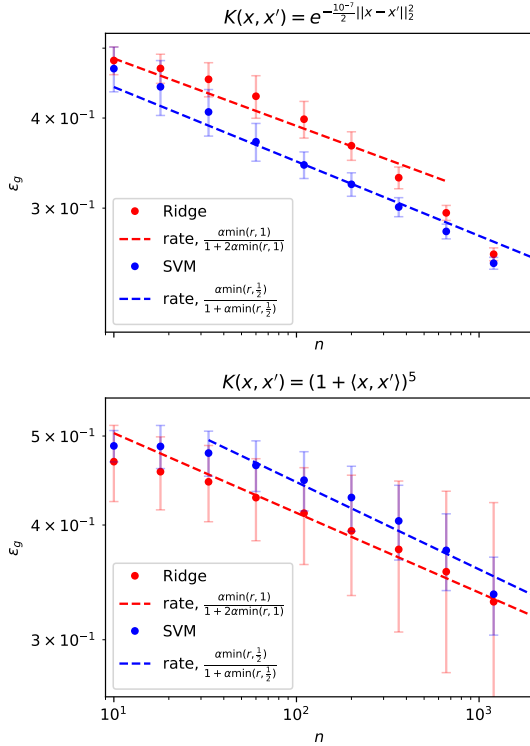


Figure 5. Dots: Misclassification error  $\epsilon_g$  of kernel classification on randomly sampled CIFAR 10 images for a RBF kernel (top) and a polynomial kernel (bottom), for max-margin SVM (blue) and optimally regularized ridge classification (red), using respectively the python `scikit-learn` `SVC` and `KernelRidge` packages. Dashed lines: Theoretical decay rates for the error  $\epsilon_g$  (16) (24), computed from empirically estimated capacity  $\alpha$  and source  $r$  coefficients (see section (5) and Appendix E for details). These coefficients were estimated to  $\alpha \approx 1.16$ ,  $r \approx 0.10$  for the RBF kernel (with corresponding rates  $a_{\text{SVM}} \approx 0.103$  for SVM and  $a_r \approx 0.093$  for ridge) and  $\alpha \approx 1.51$ ,  $r \approx 0.07$  for the polynomial kernel (with corresponding rates  $a_{\text{SVM}} \approx 0.095$  for SVM and  $a_r \approx 0.086$  for ridge), see Appendix E.

The source and capacity condition (8) provide a simple framework to study a large class of structured datasets. While idealized, we observe, similarly to (Cui et al., 2021), that some real datasets seem to fall under this category of

datasets, and hence display learning curves which are to a good degree described by the rates (16) for SVM and (24) for ridge classification.

We present as an example of such data a dataset composed of  $10^4$  randomly sampled CIFAR 10 images, where labels  $+1$  (resp.  $-1$ ) were assigned to images of animals (resp. means of transport). On the one hand, the learning curves for max-margin classification and optimally regularized ridge classification were obtained using the python `scikit-learn` `SVC`, `KernelRidge` packages. On the other hand, the spectrum  $\{\omega_k\}_k$  of the data covariance  $\Sigma$  in feature space was computed, and a teacher  $\theta^*$  providing perfect classification of the dataset was fitted using margin-maximizing SVM. Then, the capacity and source coefficients  $\alpha$ ,  $r$  (8) were estimated for the dataset by fitting  $\{\omega_k\}_k$  and  $\{\theta_k^*\}_k$  by power laws, and the theoretical rates (16) and (24) computed therefrom. More details on this method, adapted from (Bordelon et al., 2020; Spigler et al., 2020), are provided in Appendix E. The results of the simulations are presented in Figure 5 and contrasted to the theoretical rates computed from the empirically evaluated source and capacity coefficients for a Radial Basis Function (RBF) kernel with inverse variance  $10^{-7}$ , and a polynomial kernel of degree 5, with overall good agreement.

## 6. Conclusion

We study the generalization error rates for kernel classification under the Gaussian design and source/capacity regularity assumptions. While extensive studies have been devoted to the regression problem, which is now rather well understood, an analysis of error rates for classification problems has hitherto proven a much more challenging task. We derive the error rates as a function of the source and capacity coefficients for two standard classification methods, margin-maximizing SVM and ridge classification, and show that SVM classification always displays faster rates.

Future work in the same direction should focus on the one hand on putting the claims of this manuscript on more rigorous grounds, and on the other hand on investigating the corresponding noisy setting, by allowing the target function to be stochastic. While we expect the methods employed in the present work, which build upon the asymptotic results of (Loureiro et al., 2021), to readily generalize, the latter setting is nevertheless anticipated to prove more analytically intricate.

**Acknowledgements—** We thank Alessandro Rudi, Vittorio Erba and Mauro Pastore for useful discussion. We acknowledge funding from the ERC under the European Union’s Horizon 2020 Research and Innovation Programme Grant Agreement 714608-SMiLe.



## References

- Advani, M. S., Saxe, A. M., and Sompolinsky, H. High-dimensional dynamics of generalization error in neural networks. *Neural Networks*, 132:428–446, 2020.
- Ardeshtir, N., Sanford, C., and Hsu, D. Support vector machines and linear regression coincide with very high-dimensional features. *ArXiv*, abs/2105.14084, 2021.
- Aubin, B., Krzakala, F., Lu, Y. M., and Zdeborová, L. Generalization error in high-dimensional perceptrons: Approaching bayes error with convex optimization. In *Advances in Neural Information Processing Systems*, volume 33, 2020.
- Bartlett, P., Long, P. M., Lugosi, G., and Tsigler, A. Benign overfitting in linear regression. *Proceedings of the National Academy of Sciences*, 117:30063 – 30070, 2020.
- Berthier, R., Bach, F., and Gaillard, P. Tight nonparametric convergence rates for stochastic gradient descent under the noiseless linear model. *ArXiv*, abs/2006.08212, 2020.
- Bordelon, B., Canatar, A., and Pehlevan, C. Spectrum dependent learning curves in kernel regression and wide neural networks. In *International Conference on Machine Learning*, pp. 1024–1034. PMLR, 2020.
- Canatar, A., Bordelon, B., and Pehlevan, C. Spectral bias and task-model alignment explain generalization in kernel regression and infinitely wide neural networks. *Nature Communications*, 12:1–12, 2021.
- Caponnetto, A. and De Vito, E. Optimal rates for the regularized least-squares algorithm. *Foundations of Computational Mathematics*, 7(3):331–368, 2007.
- Caponnetto, A. and Vito, E. D. Fast rates for regularized least-squares algorithm. In ., 2005.
- Chizat, L., Oyallon, E., and Bach, F. On lazy training in differentiable programming. In Wallach, H., Larochelle, H., Beygelzimer, A., d'Alché-Buc, F., Fox, E., and Garnett, R. (eds.), *Advances in Neural Information Processing Systems*, volume 32. Curran Associates, Inc., 2019.
- Cortes, C. and Vapnik, V. N. Support-vector networks. *Machine Learning*, 20:273–297, 2004.
- Cui, H., Loureiro, B., Krzakala, F., and Zdeborová, L. Generalization error rates in kernel regression: The crossover from the noiseless to noisy regime. *ArXiv*, abs/2105.15004, 2021.
- Dicker, L. H. et al. Ridge regression and asymptotic minimax estimation over spheres of growing dimension. *Bernoulli*, 22(1):1–37, 2016.
- Dietrich, R., Oppen, M., and Sompolinsky, H. Statistical mechanics of support vector networks. *Physical Review Letters*, 82:2975–2978, 1999a.
- Dietrich, R., Oppen, M., and Sompolinsky, H. Statistical mechanics of support vector networks. *Physical review letters*, 82(14):2975, 1999b.
- Dobriban, E. and Wager, S. High-dimensional asymptotics of prediction: Ridge regression and classification. *The Annals of Statistics*, 46(1):247–279, 2018.
- Drucker, H., Burges, C. J. C., Kaufman, L., Smola, A., and Vapnik, V. N. Support vector regression machines. In *NIPS*, 1996.
- Engel, A. and Van den Broeck, C. *Statistical mechanics of learning*. Cambridge University Press, 2001.
- Fischer, S. and Steinwart, I. Sobolev norm learning rates for regularized least-squares algorithms. *Journal of Machine Learning Research*, 21(205):1–38, 2020.
- Hsu, D., Kakade, S. M., and Zhang, T. Random design analysis of ridge regression. In Mannor, S., Srebro, N., and Williamson, R. C. (eds.), *Proceedings of the 25th Annual Conference on Learning Theory*, volume 23 of *Proceedings of Machine Learning Research*, pp. 9.1–9.24, Edinburgh, Scotland, 25–27 Jun 2012. JMLR Workshop and Conference Proceedings.
- Hsu, D., Muthukumar, V., and Xu, J. On the proliferation of support vectors in high dimensions, 2020.
- Jacot, A., Gabriel, F., and Hongler, C. Neural tangent kernel: Convergence and generalization in neural networks. In *Advances in neural information processing systems*, pp. 8571–8580, 2018.
- Jin, H., Banerjee, P. K., and Montúfar, G. Learning curves for gaussian process regression with power-law priors and targets, 2021.
- Jun, K.-S., Cutkosky, A., and Orabona, F. Kernel truncated randomized ridge regression: Optimal rates and low noise acceleration. In *NeurIPS*, 2019.
- Krzyżak, A. The rates of convergence of kernel regression estimates and classification rules. *IEEE Trans. Inf. Theory*, 32:668–679, 1986.
- Lee, J., Bahri, Y., Novak, R., Schoenholz, S. S., Pennington, J., and Sohl-Dickstein, J. Deep neural networks as Gaussian processes, 2018. ICLR 2018, arXiv:1711.00165.
- Lin, J., Rudi, A., Rosasco, L., and Cevher, V. Optimal rates for spectral algorithms with least-squares regression over hilbert spaces. *Applied and Computational Harmonic Analysis*, 48:868–890, 2018.

- Liu, F., Liao, Z., and Suykens, J. A. Kernel regression in high dimension: Refined analysis beyond double descent. *arXiv preprint arXiv:2010.02681*, 2020.
- Loureiro, B., Gerbelot, C., Cui, H., Goldt, S., Krzakala, F., Mézard, M., and Zdeborová, L. Capturing the learning curves of generic features maps for realistic data sets with a teacher-student model. *ArXiv*, abs/2102.08127, 2021.
- Marteau-Ferey, U., Ostrovskii, D., Bach, F. R., and Rudi, A. Beyond least-squares: Fast rates for regularized empirical risk minimization through self-concordance. In *COLT*, 2019.
- Mézard, M. and Montanari, A. *Information, physics, and computation*. Oxford University Press, 2009.
- Mézard, M., Parisi, G., and Virasoro, M. *Spin glass theory and beyond: An Introduction to the Replica Method and Its Applications*, volume 9. World Scientific Publishing Company, 1987.
- Muthukumar, V., Narang, A., Subramanian, V., Belkin, M., Hsu, D., and Sahai, A. Classification vs regression in overparameterized regimes: Does the loss function matter? *Journal of Machine Learning Research*, 22(222): 1–69, 2021.
- Nadaraja, E. A. On a regression estimate. *Teor. Veroyatnost. i Primenen.*, 9:157–159, 1964. ISSN 0040-361x.
- Neal, R. M. *Priors for Infinite Networks*, pp. 29–53. Springer New York, New York, NY, 1996. ISBN 978-1-4612-0745-0. doi: 10.1007/978-1-4612-0745-0\_2.
- Oppen, M. and Urbanczik, R. Universal learning curves of support vector machines. *Phys. Rev. Lett.*, 86:4410–4413, May 2001. doi: 10.1103/PhysRevLett.86.4410.
- Pillaud-Vivien, L., Rudi, A., and Bach, F. Statistical optimality of stochastic gradient descent on hard learning problems through multiple passes. In *Advances in Neural Information Processing Systems*, volume 31, pp. 8114–8124, 2018.
- Sollich, P. and Halees, A. Learning curves for gaussian process regression: Approximations and bounds. *Neural computation*, 14(6):1393–1428, 2002.
- Spigler, S., Geiger, M., and Wyart, M. Asymptotic learning curves of kernel methods: empirical data versus teacher–student paradigm. *Journal of Statistical Mechanics: Theory and Experiment*, 2020(12):124001, 2020.
- Steinwart, I., Hush, D. R., Scovel, C., et al. Optimal rates for regularized least squares regression. In *COLT*, pp. 79–93, 2009.
- Vapnik, V. N., Golowich, S. E., and Smola, A. Support vector method for function approximation, regression estimation and signal processing. In *NIPS*, 1996.
- Varre, A., Pillaud-Vivien, L., and Flammarion, N. Last iterate convergence of sgd for least-squares in the interpolation regime. *ArXiv*, abs/2102.03183, 2021.
- Watson, G. S. Smooth regression analysis. *Sankhyā: The Indian Journal of Statistics, Series A (1961-2002)*, 26(4): 359–372, 1964. ISSN 0581572X.
- Williams, C. K. I. Computing with infinite networks. In *Proceedings of the 9th International Conference on Neural Information Processing Systems*, NIPS’96, pp. 295–301, Cambridge, MA, USA, 1996. MIT Press.

## A. Rates for margin maximizing SVM

In this appendix, we provide some analytical discussion of the equations (14) motivating the scaling (16) and (15). We remind the risk for the hinge loss (13)

$$\hat{\mathcal{R}}_n(w) = \frac{1}{n} \sum_{\mu=1}^n \max(0, 1 - y^\mu w^\top \psi(x)) + \lambda w^\top w, \quad (26)$$

with  $\lambda = 0^+$  for max-margin. The predictor is then  $\hat{y} = \text{sign}(\hat{w} \cdot \psi(x))$ .

### A.1. Mapping from (Loureiro et al., 2021)

The starting point is the closed-form asymptotic characterization of the misclassification error of (Loureiro et al., 2021). We begin by reviewing the main results of (Loureiro et al., 2021), and detail how their setting can be mapped to ours. Consider hinge regression on  $n$  independent  $p$ -dimensional Gaussian samples  $\mathcal{D} = \{x^\mu, y^\mu\}_{\mu=1}^n$ , by minimizing the empirical risk

$$\hat{\mathcal{R}}_n(w) = \sum_{\mu=1}^n \max\left(0, 1 - y^\mu \frac{w^\top x^\mu}{\sqrt{p}}\right) + \frac{\lambda}{2} w^\top w. \quad (27)$$

for some constant regularization strength  $\lambda \geq 0$ . Suppose that the labels are generated from a teacher/target/oracle  $\theta^* \in \mathbb{R}^p$  as  $y^\mu = \text{sign}(\theta^{*\top} x^\mu)$ . Then provided the assumptions

**Assumption A.1.**  $n \gg 1$ ,  $p \gg 1$ ,  $\frac{n}{p} = \mathcal{O}(1)$ ,

**Assumption A.2.**  $0 < \frac{1}{p} \|\theta^*\|_2^2 < \infty$ ,

are satisfied, there exist constants  $C, c, c' > 0$  so that for all  $0 < \epsilon < c'$ ,

$$\mathbb{P}\left(\left|\epsilon_g - \frac{1}{\pi} \arccos\left(\frac{m^*}{\sqrt{\rho q^*}}\right)\right| > \epsilon\right) < \frac{C}{\epsilon} e^{-cn\epsilon^2}, \quad (28)$$

where  $\rho = \theta^{*\top} \Sigma \theta^* / p$  and  $m^*, q^*$  are the solutions of the *fixed point equations*

$$\begin{cases} m = \frac{\hat{m}}{p} \text{tr} \frac{\Sigma \theta^* \theta^{*\top} \Sigma}{\lambda + \hat{V} \Sigma} \\ q = \frac{1}{p} \text{tr} \frac{\hat{m}^2 \Sigma \theta^* \theta^{*\top} \Sigma^2 + \hat{q} \Sigma^2}{(\lambda + \hat{V} \Sigma)^2} \\ V = \frac{1}{p} \text{tr} \frac{\Sigma}{\lambda + \hat{V} \Sigma} \\ \hat{m} = \frac{\frac{n}{p}}{V \sqrt{\rho}} \frac{1}{2\pi} \left\{ \sqrt{2\pi} \left[ \text{erf}\left(\frac{1}{\sqrt{2q(1-\eta)}}\right) - \text{erf}\left(\frac{1-V}{\sqrt{2q(1-\eta)}}\right) \right] \right. \\ \quad \left. + 2\sqrt{q(1-\eta)} \left( e^{-\frac{1}{2q(1-\eta)}} - e^{-\frac{(1-V)^2}{2q(1-\eta)}} \right) + \sqrt{2\pi} V \left( 1 + \text{erf}\left(\frac{1-V}{\sqrt{2q(1-\eta)}}\right) \right) \right\} \\ \hat{q} = \frac{n}{p} \left[ \int_{-\infty}^{\frac{1-V}{\sqrt{q}}} dx \frac{e^{-\frac{1}{2}x^2}}{\sqrt{2\pi}} \left[ 1 + \text{erf}\left(\sqrt{\frac{\eta}{2(1-\eta)}} x\right) \right] + \frac{1}{V^2} \int_{\frac{1-V}{\sqrt{q}}}^{\frac{1}{\sqrt{q}}} dx \frac{e^{-\frac{1}{2}x^2}}{\sqrt{2\pi}} \left[ 1 + \text{erf}\left(\sqrt{\frac{\eta}{2(1-\eta)}} x\right) \right] (1 - \sqrt{q}x)^2 \right] \\ \hat{V} = \frac{n}{p} \int_{\frac{1-V}{\sqrt{q}}}^{\frac{1}{\sqrt{q}}} dx \frac{e^{-\frac{1}{2}x^2}}{\sqrt{2\pi}} \left[ 1 + \text{erf}\left(\sqrt{\frac{\eta}{2(1-\eta)}} x\right) \right] \end{cases},$$

with  $\eta = m^2/(\rho q)$ , and  $\Sigma$  the covariance of the samples  $x$ . The limit  $\lambda = 0^+$  can be taken using the rescaling (Aubin et al., 2020)

$$\hat{m} \leftarrow \frac{\hat{m}}{\lambda}, \quad \hat{q} \leftarrow \frac{\hat{q}}{\lambda}, \quad \hat{V} \leftarrow \frac{\hat{V}}{\lambda}, \quad V \leftarrow \lambda V. \quad (29)$$

The equations (29) simplify in this limit to

$$\begin{cases} m = \frac{\hat{m}}{p} \text{tr} \frac{\Sigma \theta^* \theta^{*\top} \Sigma}{1 + \hat{V} \Sigma} \\ q = \frac{1}{p} \text{tr} \frac{\hat{m}^2 \Sigma \theta^* \theta^{*\top} \Sigma^2 + \hat{q} \Sigma^2}{(1 + \hat{V} \Sigma)^2} \\ V = \frac{1}{p} \text{tr} \frac{\Sigma}{1 + \hat{V} \Sigma} \end{cases}, \quad \begin{cases} \hat{m} = \frac{\frac{n}{p}}{\sqrt{\rho}} \frac{1}{2\pi} \left( \sqrt{2\pi} (1 + \text{erf}(\frac{1}{\sqrt{2q(1-\eta)}})) + 2e^{-\frac{1}{2q(1-\eta)}} \sqrt{q(1-\eta)} \right) \\ \hat{q} = \frac{\frac{n}{p}}{\hat{V}^2} \int_{-\infty}^{\frac{1}{\sqrt{q}}} dx \frac{e^{-\frac{1}{2}x^2}}{\sqrt{2\pi}} \left[ 1 + \text{erf}(\sqrt{\frac{\eta}{2(1-\eta)}} x) \right] (1 - \sqrt{q}x)^2 \\ \hat{V} = \frac{\frac{n}{p}}{\hat{V}} \int_{-\infty}^{\frac{1}{\sqrt{q}}} dx \frac{e^{-\frac{1}{2}x^2}}{\sqrt{2\pi}} \left[ 1 + \text{erf}(\sqrt{\frac{\eta}{2(1-\eta)}} x) \right] \end{cases}. \quad (30)$$

Note that the risk studied by (Loureiro et al., 2021) (27) differs from the one we consider (13) by the scaling  $1/\sqrt{p}$ , the missing  $1/n$  in front of the sum, and a factor 2 for the regularization strength. All those scalings can be absorbed in  $\lambda \leftarrow 2\lambda/n$  and  $\Sigma \leftarrow \Sigma/p$ , leading to (14):

$$\begin{cases} m = \hat{m} p \text{tr} \frac{\Sigma \theta^* \theta^{*\top} \Sigma}{1 + \hat{V} \Sigma} \\ q = p \text{tr} \frac{\hat{m}^2 \Sigma \theta^* \theta^{*\top} \Sigma^2 + \hat{q} \Sigma^2}{(1 + \hat{V} \Sigma)^2} \\ V = \text{tr} \frac{\Sigma}{1 + \hat{V} \Sigma} \end{cases}, \quad \begin{cases} \hat{m} = \frac{\frac{n}{p}}{\sqrt{\rho}} \frac{1}{2\pi} \left( \sqrt{2\pi} (1 + \text{erf}(\frac{1}{\sqrt{2q(1-\eta)}})) + 2e^{-\frac{1}{2q(1-\eta)}} \sqrt{q(1-\eta)} \right) \\ \hat{q} = \frac{\frac{n}{p}}{\hat{V}^2} \int_{-\infty}^{\frac{1}{\sqrt{q}}} dx \frac{e^{-\frac{1}{2}x^2}}{\sqrt{2\pi}} \left[ 1 + \text{erf}(\sqrt{\frac{\eta}{2(1-\eta)}} x) \right] (1 - \sqrt{q}x)^2 \\ \hat{V} = \frac{\frac{n}{p}}{\hat{V}} \int_{-\infty}^{\frac{1}{\sqrt{q}}} dx \frac{e^{-\frac{1}{2}x^2}}{\sqrt{2\pi}} \left[ 1 + \text{erf}(\sqrt{\frac{\eta}{2(1-\eta)}} x) \right] \end{cases}, \quad (31)$$

thereby completing the mapping from the setup in (Loureiro et al., 2021) to the present setting. Note importantly that these two rescalings, along the  $1 \ll n \ll p = \infty$  limit considered in this work, mean that we employ the equations (29) outside of the asymptotic regime for which they were proven. However, the results of (Cui et al., 2021) suggest that these equations still hold and stand in very good agreement with numerical simulations. A rigorous proof of the following analysis falls out of the scope of the present work and is left for future analysis.

## A.2. Equations for max-margin under source and capacity conditions

In the following, we detail the asymptotic scaling analysis of the equations (14). For a diagonal covariance  $\Sigma = \text{diag}(\omega_1, \dots, \omega_p)$  and  $\theta^* = (\theta_k^*)_k$ , (14) reads

$$\begin{cases} \rho = \sum_{k=1}^p \theta_k^{*2} \omega_k \\ m = \hat{m} p \sum_{k=1}^d \frac{\omega_k^2 \theta_k^{*2}}{1 + \hat{V} p \omega_k} \\ q = p \sum_{k=1}^p \frac{\hat{m}^2 \theta_k^{*2} \omega_k^3 + \hat{q} \omega_k^2}{(1 + \hat{V} p \omega_k)^2} \\ V = \sum_{k=1}^p \frac{\omega_k}{1 + \hat{V} p \omega_k} \end{cases}, \quad \begin{cases} \hat{m} = \frac{\frac{n}{p}}{\sqrt{\rho}} \frac{1}{2\pi} \left( \sqrt{2\pi} (1 + \text{erf}(\frac{1}{\sqrt{2q(1-\eta)}})) + 2e^{-\frac{1}{2q(1-\eta)}} \sqrt{q(1-\eta)} \right) \\ \hat{q} = \frac{\frac{n}{p}}{\hat{V}^2} \int_{-\infty}^{\frac{1}{\sqrt{q}}} dx \frac{e^{-\frac{1}{2}x^2}}{\sqrt{2\pi}} \left[ 1 + \text{erf}(\sqrt{\frac{\eta}{2(1-\eta)}} x) \right] (1 - \sqrt{q}x)^2 \\ \hat{V} = \frac{\frac{n}{p}}{\hat{V}} \int_{-\infty}^{\frac{1}{\sqrt{q}}} dx \frac{e^{-\frac{1}{2}x^2}}{\sqrt{2\pi}} \left[ 1 + \text{erf}(\sqrt{\frac{\eta}{2(1-\eta)}} x) \right] \end{cases}. \quad (32)$$

To simplify the equations (32), we introduce the auxiliary variables  $z = \frac{n}{p}/\hat{V}$ ,  $\hat{r}_1 = \hat{m}/\hat{V}$  and  $\hat{r}_2 = (n\hat{q})/(p\hat{V}^2)$ . The intuitive meaning of  $z$  is loosely that of an effective regularization. In the context of kernel ridge *regression* where a similar variable appears, the role of  $z$  as an effective regularizing term is quite clear in (Cui et al., 2021). We also refer the reader to the discussion in (Loureiro et al., 2021), also for ridge regression, where the role of  $\hat{V}$  as parametrizing the gap between training and test error is mentioned.  $\hat{r}_1$  is to be regarded as the ratio between the norm of the estimator  $\hat{w}$  minimizing the

risk (13), and the norm of the teacher  $\theta^*$ . Introducing these variables in (32) allows to have a well defined  $p = \infty$  limit, which reads

$$\left\{ \begin{array}{l} \rho = \sum_{k=1}^{\infty} \theta_k^{*2} \omega_k \\ m = \hat{r}_1 \frac{n}{z} \sum_{k=1}^{\infty} \frac{\omega_k^2 \theta_k^{*2}}{1 + \frac{n}{z} \omega_k} \\ q = \frac{n^2}{z^2} \sum_{k=1}^{\infty} \frac{\hat{r}_1^2 \theta_k^{*2} \omega_k^3 + \frac{1}{n} \hat{r}_2 \omega_k^2}{(1 + \frac{n}{z} \omega_k)^2} \\ V = \sum_{k=1}^d \frac{\omega_k}{1 + \frac{n}{z} \omega_k} \end{array} \right. , \quad \left\{ \begin{array}{l} \hat{r}_1 = \frac{\hat{m}}{\hat{V}} = \frac{1}{2\pi\sqrt{\rho}} \frac{\left( \sqrt{2\pi}(1 + \operatorname{erf}(\frac{1}{\sqrt{2q(1-\eta)}})) + 2e^{-\frac{1}{2q(1-\eta)}} \sqrt{q(1-\eta)} \right)}{\int_{-\infty}^{\frac{1}{\sqrt{q}}} dx \frac{e^{-\frac{1}{2}x^2}}{\sqrt{2\pi}} [1 + \operatorname{erf}(\sqrt{\frac{\eta}{2(1-\eta)}}x)]} \\ \hat{r}_2 = \frac{\frac{n}{p} \hat{q}}{\hat{V}^2} = \frac{\int_{-\infty}^{\frac{1}{\sqrt{q}}} dx \frac{e^{-\frac{1}{2}x^2}}{\sqrt{2\pi}} [1 + \operatorname{erf}(\sqrt{\frac{\eta}{2(1-\eta)}}x)] (1 - \sqrt{q}x)^2}{\left( \int_{-\infty}^{\frac{1}{\sqrt{q}}} dx \frac{e^{-\frac{1}{2}x^2}}{\sqrt{2\pi}} [1 + \operatorname{erf}(\sqrt{\frac{\eta}{2(1-\eta)}}x)] \right)^2} \end{array} \right. . \quad (33)$$

From (32),  $z$  satisfies the self-consistent equation

$$z = \frac{\frac{z}{n} \sum_{k=1}^{\infty} \frac{\omega_k}{\frac{z}{n} + \omega_k}}{\int_{-\infty}^{\frac{1}{\sqrt{q}}} dx \frac{e^{-\frac{1}{2}x^2}}{\sqrt{2\pi}} [1 + \operatorname{erf}(\sqrt{\frac{\eta}{2(1-\eta)}}x)]} \approx \frac{\left(\frac{z}{n}\right)^{1-\frac{1}{\alpha}} \int_{\left(\frac{z}{n}\right)^{\frac{1}{\alpha}}}^{\infty} \frac{dx}{1+x^\alpha}}{\int_{-\infty}^{\frac{1}{\sqrt{q}}} dx \frac{e^{-\frac{1}{2}x^2}}{\sqrt{2\pi}} [1 + \operatorname{erf}(\sqrt{\frac{\eta}{2(1-\eta)}}x)]} , \quad (34)$$

where a Riemann approximation of the sum was used. We introduce its to-be-determined scaling  $\gamma$ ,

$$z \sim C_z n^{1-\alpha\gamma}, \quad (35)$$

where  $C_z$  designates the prefactor. In the following, we discuss the scaling and the corrections of the order parameters and express them as a function of  $\gamma$ , before determining its value using the numerical solution of (33). Note that the scaling (35) implies in particular the following scaling for the integral

$$\int_{-\infty}^{\frac{1}{\sqrt{q}}} dx \frac{e^{-\frac{1}{2}x^2}}{\sqrt{2\pi}} [1 + \operatorname{erf}(\sqrt{\frac{\eta}{2(1-\eta)}}x)] \sim n^{\gamma-1}. \quad (36)$$

### A.3. First order corrections

We now plug the source and capacity ansatz (7) into the equations (33)

$$\omega_k \sim k^{-\alpha}, \quad \theta_k^* \sim k^{-\frac{1+\alpha(2r-1)}{2}}, \quad (37)$$

yielding

$$\left\{ \begin{array}{l} \rho = \sum_{k=1}^{\infty} k^{-1-2\alpha r} \\ m = \hat{r}_1 \sum_{k=1}^{\infty} \frac{k^{-1-2\alpha r}}{1 + \frac{z}{n} k^\alpha} \\ q = \hat{r}_1^2 \sum_{k=1}^{\infty} \frac{k^{-1-2\alpha r}}{(1 + \frac{z}{n} k^\alpha)^2} + \frac{\hat{r}_2}{n} \sum_{k=1}^{\infty} \frac{1}{(1 + \frac{z}{n} k^\alpha)^2} \\ V = \frac{z}{n} \sum_{k=1}^{\infty} \frac{1}{1 + \frac{z}{n} k^\alpha} \end{array} \right. , \quad \left\{ \begin{array}{l} \hat{r}_1 = \frac{1}{2\pi\sqrt{\rho}} \frac{\left( \sqrt{2\pi}(1 + \operatorname{erf}(\frac{1}{\sqrt{2q(1-\eta)}})) + 2e^{-\frac{1}{2q(1-\eta)}} \sqrt{q(1-\eta)} \right)}{\int_{-\infty}^{\frac{1}{\sqrt{q}}} dx \frac{e^{-\frac{1}{2}x^2}}{\sqrt{2\pi}} [1 + \operatorname{erf}(\sqrt{\frac{\eta}{2(1-\eta)}}x)]} \\ \hat{r}_2 = \frac{\int_{-\infty}^{\frac{1}{\sqrt{q}}} dx \frac{e^{-\frac{1}{2}x^2}}{\sqrt{2\pi}} [1 + \operatorname{erf}(\sqrt{\frac{\eta}{2(1-\eta)}}x)] (1 - \sqrt{q}x)^2}{\left( \int_{-\infty}^{\frac{1}{\sqrt{q}}} dx \frac{e^{-\frac{1}{2}x^2}}{\sqrt{2\pi}} [1 + \operatorname{erf}(\sqrt{\frac{\eta}{2(1-\eta)}}x)] \right)^2} \end{array} \right. . \quad (38)$$

Massaging the expression for  $m$  (and remembering  $z \sim n^{1-\alpha\gamma}$  (35))



$$\begin{aligned}
 m &= \hat{r}_1 \rho - \hat{r}_1 \sum_{k=1}^{\infty} \frac{k^{-1-2\alpha r} C_z \left(\frac{k}{n^\gamma}\right)^\alpha}{1 + C_z \left(\frac{k}{n^\gamma}\right)^\alpha} \\
 &= \hat{r}_1 \rho - C_z \hat{r}_1 n^{-\gamma\alpha} \sum_{k=1}^{\infty} \frac{k^{-1-2\alpha(r-\frac{1}{2})}}{1 + C_z \left(\frac{k}{n^\gamma}\right)^\alpha} \\
 &\approx \hat{r}_1 \rho - \mathbb{1}_{r \geq \frac{1}{2}} \hat{r}_1 C_z \left[ n^{-\gamma\alpha} \sum_{k=1}^{n^\gamma} \frac{k^{-1-2\alpha(r-\frac{1}{2})}}{1 + C_z \left(\frac{k}{n^\gamma}\right)^\alpha} + n^{-2\gamma\alpha r} \int_1^{\infty} \frac{x^{-1+\alpha(1-2r)}}{1 + C_z x^\alpha} \right] - \mathbb{1}_{r \leq \frac{1}{2}} C_z \hat{r}_1 n^{-2\gamma\alpha r} \int_0^{\infty} \frac{x^{-1+\alpha(1-2r)}}{1 + C_z x^\alpha} \\
 &= \hat{r}_1 \left[ \rho - \mathbb{1}_{r \geq \frac{1}{2}} C_z A_m^n n^{-\gamma\alpha} - C_z n^{-2\gamma\alpha r} \int_{\Theta(r-\frac{1}{2})}^{\infty} \frac{x^{-1+\alpha(1-2r)}}{1 + C_z x^\alpha} \right] + o\left(\max\left(n^{-\gamma\alpha}, n^{-2\gamma\alpha r}\right)\right), \tag{39}
 \end{aligned}$$

where we used the shorthand

$$A_m^n \stackrel{\text{def}}{=} \sum_{k=1}^{n^\gamma} \frac{k^{-1-2\alpha(r-\frac{1}{2})}}{1 + C_z \left(\frac{k}{n^\gamma}\right)^\alpha}. \tag{40}$$

Massaging by the same token the equation for  $q$ ,

$$\begin{aligned}
 q &\approx \hat{r}_1^2 \rho - \hat{r}_1^2 \sum_{k=1}^{\infty} \frac{k^{-1-2\alpha r} \left(C_z^2 \left(\frac{k}{n^\gamma}\right)^{2\alpha} + 2C_z \left(\frac{k}{n^\gamma}\right)^\alpha\right)}{\left(1 + C_z \left(\frac{k}{n^\gamma}\right)^\alpha\right)^2} + \hat{r}_2 n^{\gamma-1} \int_0^{\infty} \frac{1}{(1 + C_z x^\alpha)^2} \\
 &\approx \hat{r}_1^2 \rho + \hat{r}_2 n^{\gamma-1} \int_0^{\infty} \frac{1}{(1 + C_z x^\alpha)^2} \\
 &\quad - 2\hat{r}_1^2 C_z \left[ \mathbb{1}_{r \geq \frac{1}{2}} \left( n^{-\gamma\alpha} \sum_{k=1}^{n^\gamma} \frac{k^{-1-2\alpha(r-\frac{1}{2})}}{\left(1 + C_z \left(\frac{k}{n^\gamma}\right)^\alpha\right)^2} + n^{-2\gamma\alpha r} \int_1^{\infty} \frac{x^{-1+\alpha(1-2r)}}{(1 + C_z x^\alpha)^2} \right) + \mathbb{1}_{r \leq \frac{1}{2}} n^{-2\gamma\alpha r} \int_0^{\infty} \frac{x^{-1+\alpha(1-2r)}}{(1 + C_z x^\alpha)^2} \right] \\
 &\quad - \hat{r}_1^2 C_z^2 \left[ \mathbb{1}_{r \geq 1} \left( n^{-2\gamma\alpha} \sum_{k=1}^{n^\gamma} \frac{k^{-1-2\alpha(r-1)}}{\left(1 + C_z \left(\frac{k}{n^\gamma}\right)^\alpha\right)^2} + n^{-2\gamma\alpha r} \int_1^{\infty} \frac{x^{-1+\alpha(2-2r)}}{(1 + C_z x^\alpha)^2} \right) + \mathbb{1}_{r \leq 1} n^{-2\gamma\alpha r} \int_0^{\infty} \frac{x^{-1+\alpha(2-2r)}}{(1 + C_z x^\alpha)^2} \right] \\
 &= \hat{r}_1^2 \left[ \rho + \frac{\hat{r}_2}{\hat{r}_1^2} n^{\gamma-1} \int_0^{\infty} \frac{1}{(1 + C_z x^\alpha)^2} - \mathbb{1}_{r \geq \frac{1}{2}} 2C_z A_q^n n^{-\gamma\alpha} - \mathbb{1}_{r \geq 1} C_z^2 B_q^n n^{-2\gamma\alpha} \right. \\
 &\quad \left. - n^{-2\gamma\alpha r} \left( 2C_z \int_{\Theta(r-\frac{1}{2})}^{\infty} \frac{x^{-1+\alpha(1-2r)}}{(1 + C_z x^\alpha)^2} + C_z^2 \int_{\Theta(r-1)}^{\infty} \frac{x^{-1+\alpha(2-2r)}}{(1 + C_z x^\alpha)^2} \right) \right] + o\left(\max\left(\frac{\hat{r}_2}{\hat{r}_1^2} n^{\gamma-1}, n^{-\gamma\alpha}, n^{-2\gamma\alpha r}\right)\right), \tag{41}
 \end{aligned}$$

where we defined

$$A_q^n \stackrel{\text{def}}{=} \sum_{k=1}^{n^\gamma} \frac{k^{-1-2\alpha(r-\frac{1}{2})}}{\left(1 + C_z \left(\frac{k}{n^\gamma}\right)^\alpha\right)^2}, \quad B_q^n \stackrel{\text{def}}{=} \sum_{k=1}^{n^\gamma} \frac{k^{-1-2\alpha(r-1)}}{\left(1 + C_z \left(\frac{k}{n^\gamma}\right)^\alpha\right)^2}. \tag{42}$$

Note that both the expansions (39) and (41) do *not* exhaustively contain all the corrections. For instance, the corrections induced by approximating Riemann sums using integrals have been omitted. More generally, getting an exhaustive and thorough asymptotic expansion out of the system of coupled equations (33) is hard, because of the coupling between the different variables. We leave such a complete analysis for future work and assume in the following that the considered corrections in (39) and (41) are the leading ones, as numerical simulations seem to back up.

An important remark on (39) and (41) is that  $A_q^m$  and  $A_m^n$  tend to the same limit as  $n \rightarrow \infty$ ,

$$A_{m,q}^\infty = \sum_{k=1}^{\infty} k^{-1-2\alpha(r-\frac{1}{2})}, \quad (43)$$

with (for  $r \geq \frac{1}{2}$  since there is an indicator function in front of  $A_{m,q}^n$ )

$$\begin{cases} n^{-\gamma\alpha} |A_m^n - A^\infty| = \frac{n^{-2\alpha\gamma r}}{2\alpha(r-\frac{1}{2})} + \mathbb{1}_{\frac{1}{2} \leq r \leq 1} C_z n^{-2\alpha\gamma r} \int_0^1 \frac{x^{-1-2\alpha(r-1)}}{1+C_z x^\alpha} + \mathbb{1}_{r \geq 1} C_z n^{-2\gamma\alpha} \sum_{k=1}^{\infty} k^{-1-2\alpha(r-1)}, \\ n^{-\gamma\alpha} |A_q^n - A^\infty| = \frac{n^{-2\alpha\gamma r}}{2\alpha(r-\frac{1}{2})} + 2\mathbb{1}_{\frac{1}{2} \leq r \leq 1} C_z n^{-2\alpha\gamma r} \int_0^1 \frac{x^{-1-2\alpha(r-1)}}{(1+C_z x^\alpha)^2} + 2\mathbb{1}_{r \geq 1} C_z n^{-2\gamma\alpha} \sum_{k=1}^{\infty} k^{-1-2\alpha(r-1)} + o(n^{-2\gamma\alpha}). \end{cases} \quad (44)$$

Again, these asymptotic expansion are not exhaustive. More straightforwardly,

$$B_q^\infty = \sum_{k=1}^{\infty} k^{-1-2\alpha(r-1)}. \quad (45)$$

Finally, remark that the expansions (39) and (41) imply that  $m \sim \hat{r}_1 \rho$  and  $q \sim \hat{r}_1^2 \rho$ , which echoes the intuitive meaning of  $m, q$  as  $\langle \hat{w}, \theta^* \rangle_{L^2(\mathcal{X})}$ ,  $\|\hat{w}\|_{L^2(\mathcal{X})}^2$  and of  $\hat{r}_1$  as  $\|\hat{w}\|_{L^2(\mathcal{X})} / \|\theta^*\|_{L^2(\mathcal{X})}^2$ , see also discussion in section 2 under equation (12).

The expansions (39) and (41) can be plugged into the expression of the cosine similarity  $\eta$  (9) to access the decay rate for the misclassification error.

$$\begin{aligned} \eta &= \frac{\left(1 - \mathbb{1}_{r \geq \frac{1}{2}} C_z \frac{A_m^n}{\rho} n^{-\gamma\alpha} - n^{-2\gamma\alpha r} \frac{C_z}{\rho} \int_{\Theta(r-\frac{1}{2})}^{\infty} \frac{x^{-1+\alpha(1-2r)}}{1+C_z x^\alpha} \right)^2}{1 + \frac{\hat{r}_2}{\rho \hat{r}_1^2} n^{\gamma-1} \int_0^{\infty} \frac{1}{(1+x^\alpha)^2} - \frac{\mathbb{1}_{r \geq \frac{1}{2}} 2C_z A_q^n n^{-\gamma\alpha} - \mathbb{1}_{r \geq 1} C_z^2 B_q^n n^{-2\gamma\alpha}}{\rho} - n^{-2\gamma\alpha r} \frac{C_z}{\rho} \left( 2 \int_{\Theta(r-\frac{1}{2})}^{\infty} \frac{x^{-1+\alpha(1-2r)}}{(1+C_z x^\alpha)^2} + C_z \int_{\Theta(r-1)}^{\infty} \frac{x^{-1+\alpha(2-2r)}}{(1+C_z x^\alpha)^2} \right)} \\ &= 1 - \mathcal{O}\left(\frac{\hat{r}_2}{\rho \hat{r}_1^2} n^{\gamma-1}\right) + \mathbb{1}_{r \geq 1} \mathcal{O}(n^{-2\gamma\alpha}) + \mathcal{O}(n^{-2\gamma\alpha r}), \end{aligned} \quad (46)$$

where we used  $A_q^\infty = A_m^\infty$ , meaning the leading order of the  $n^{-\gamma\alpha}$  term cancels out. The scaling of the other order parameters  $q, m, \hat{r}_1, \hat{r}_2$  can at this point also be deduced. To see how, notice that

$$\int_{-\infty}^{\frac{1}{\sqrt{q}}} dx \frac{e^{-\frac{1}{2}x^2}}{\sqrt{2\pi}} \left[ 1 + \operatorname{erf}\left(\sqrt{\frac{\eta}{2(1-\eta)}} x\right) \right] \approx \frac{1}{\sqrt{q}} \int_{-\infty}^1 dx \frac{e^{-\frac{x^2}{2q}}}{\sqrt{2\pi}} \left[ 1 + \operatorname{erf}\left(\sqrt{\frac{\eta}{2q(1-\eta)}} x\right) \right] \sim \frac{1}{\sqrt{q}}, \quad (47)$$

which together with the observation (36) implies

$$q \sim \hat{r}_1^2 \sim n^{2(1-\gamma)}. \quad (48)$$

In parallel, it follows from a similar change of variables in the expression of  $\hat{r}_2$  that

$$\hat{r}_2 \sim \sqrt{q} \sim \hat{r}_1 \sim n^{1-\gamma}. \quad (49)$$

Then, returning to (46),

$$1 - \eta = \mathcal{O}(n^{2(\gamma-1)}) + \mathbb{1}_{r \geq 1} \mathcal{O}(n^{-2\gamma\alpha}) + \mathcal{O}(n^{-2\gamma\alpha r}). \quad (50)$$

The final step is to guess the value for  $\gamma$ , as a complete asymptotic analysis of the system (33) to rigorously close the equations is out of the scope of the present paper. A naive motivation to find  $\gamma$  can be the following : suppose the dominating rate in (41) is  $2(\gamma-1)$ . Since from the physical meaning of the order parameters (12) it is reasonable to expect the leading

corrections of  $m$  and  $q$  to share the same decay rate, and since the leading corrections of  $m$  has rate  $-2\gamma\alpha\min(r, 1/2)$ , a guess for  $\gamma$  following from equating the two rates is

$$\gamma = \frac{1}{1 + \alpha\min(r, \frac{1}{2})}. \quad (51)$$

This guess compares very well with numerical simulations, and with the numerical solution of (33), see Fig. 1. Another argument for the formula (51) is numerical : from numerical simulations of the system (33) using the `g3m` package of (Loureiro et al., 2021), it appears the first corrections of  $(m - \hat{r}_1\rho)/\hat{r}_1\rho$  and  $(q - \hat{r}_1^2\rho)/2\hat{r}_1^2\rho$  have the same decay rate but are not equal. From the expansion (39), for  $r > 1/2$ , the leading correction of  $(m - \hat{r}_1\rho)/\hat{r}_1\rho$  has decay rate  $-\gamma\alpha$ , with prefactor  $C_z A_m^\infty/\rho$ . But the correction of rate  $-\gamma\alpha$  in  $(q - \hat{r}_1^2\rho)/2\hat{r}_1^2\rho$  has the same prefactor, as  $A_q^\infty = A_m^\infty$ . Since the prefactors are not observed to be equal, it must be that another term in the expansion (41) has also rate  $-\gamma\alpha$ , with the only possibility being the term with rate  $2(\gamma - 1)$ . Equating the two rates allows to recover (51) for  $r > 1/2$ .

Assuming (51) to be true, since  $\epsilon_g = \cos^{-1}(\eta) \sim \sqrt{1 - \eta}$ ,

$$\epsilon_g \sim n^{-\gamma\alpha\min(r, \frac{1}{2})} = n^{-\frac{\alpha\min(r, \frac{1}{2})}{1 + \alpha\min(r, \frac{1}{2})}}, \quad (52)$$

which is the error rate for max-margin classification (16).

## B. Rates for regularized hinge classification

In this Appendix, we show that margin-maximizing SVM is optimal for classifying teachers with source  $r \leq \frac{1}{2}$ , i.e. in  $L^2(\mathcal{X}) \setminus \mathcal{H}$ , and argue why this is also expected to extend to teachers in  $\mathcal{H}$ . In other words, we give evidence that the optimal regularization in the hinge classification risk (13) on the dataset (8) is for vanishing  $\lambda = 0$ . To this end, we derive the rates for the misclassification error of ERM on (13) for generic regularization  $\lambda$ , building upon the results of (Loureiro et al., 2021) in similar fashion to Appendix A.

### B.1. Regularized hinge classification under source and capacity conditions

We remind the fixed point equations for the risk (13) (see Appendix A):

$$\begin{cases} m = \hat{m}p \operatorname{tr} \frac{\Sigma \theta^* \theta^{*\top} \Sigma}{\frac{n\lambda}{2} + p\hat{V}\Sigma} \\ q = p \operatorname{tr} \frac{p\hat{m}^2 \Sigma \theta^* \theta^{*\top} \Sigma^2 + \hat{q}\Sigma^2}{(\frac{n\lambda}{2} + p\hat{V}\Sigma)^2} \\ V = \operatorname{tr} \frac{\Sigma}{\frac{n\lambda}{2} + p\hat{V}\Sigma} \\ \hat{m} = \frac{\frac{n}{p}}{V\sqrt{\rho}} \frac{1}{2\pi} \left\{ \sqrt{2\pi} \left[ \operatorname{erf} \left( \frac{1}{\sqrt{2q(1-\eta)}} \right) - \operatorname{erf} \left( \frac{1-V}{\sqrt{2q(1-\eta)}} \right) \right] \right. \\ \quad \left. + 2\sqrt{q(1-\eta)} \left( e^{-\frac{1}{2q(1-\eta)}} - e^{-\frac{(1-V)^2}{2q(1-\eta)}} \right) + \sqrt{2\pi} V \left( 1 + \operatorname{erf} \left( \frac{1-V}{\sqrt{2q(1-\eta)}} \right) \right) \right\} \\ \hat{q} = \frac{n}{p} \left[ \int_{-\infty}^{\frac{1-V}{\sqrt{q}}} dx \frac{e^{-\frac{1}{2}x^2}}{\sqrt{2\pi}} \left[ 1 + \operatorname{erf} \left( \sqrt{\frac{\eta}{2(1-\eta)}} x \right) \right] + \frac{1}{V^2} \int_{\frac{1-V}{\sqrt{q}}}^{\frac{1}{\sqrt{q}}} dx \frac{e^{-\frac{1}{2}x^2}}{\sqrt{2\pi}} \left[ 1 + \operatorname{erf} \left( \sqrt{\frac{\eta}{2(1-\eta)}} x \right) \right] (1 - \sqrt{q}x)^2 \right] \\ \hat{V} = \frac{n}{p} \int_{\frac{1-V}{\sqrt{q}}}^{\frac{1}{\sqrt{q}}} dx \frac{e^{-\frac{1}{2}x^2}}{\sqrt{2\pi}} \left[ 1 + \operatorname{erf} \left( \sqrt{\frac{\eta}{2(1-\eta)}} x \right) \right] \end{cases}. \quad (53)$$

Introducing the effective regularization  $z = \frac{\alpha n \lambda}{2V}$ , satisfying

$$z = \frac{\frac{z}{n} \sum_{k=1}^{\infty} \frac{\lambda_k}{\frac{z}{n} + \lambda_k}}{\int_{\frac{1-V}{\sqrt{q}}}^{\frac{1}{\sqrt{q}}} dx \frac{e^{-\frac{1}{2}x^2}}{\sqrt{2\pi}} \left[1 + \operatorname{erf}\left(\sqrt{\frac{\eta}{2(1-\eta)}}x\right)\right]} \approx \frac{\left(\frac{z}{n}\right)^{1-\frac{1}{\alpha}} \int_{\left(\frac{z}{n}\right)^{\frac{1}{\alpha}}}^{\infty} \frac{dx}{1+x^\alpha}}{\int_{\frac{1-V}{\sqrt{q}}}^{\frac{1}{\sqrt{q}}} dx \frac{e^{-\frac{1}{2}x^2}}{\sqrt{2\pi}} \left[1 + \operatorname{erf}\left(\sqrt{\frac{\eta}{2(1-\eta)}}x\right)\right]}, \quad (54)$$

the equations (53) can be rewritten as

$$\begin{cases} \rho = \sum_{k=1}^{\infty} \theta_k^2 \lambda_k \\ m = \hat{r}_1 \frac{n}{z} \sum_{k=1}^{\infty} \frac{\lambda_k^2 \theta_k^2}{1 + \frac{n}{z} \lambda_k} \\ q = \frac{n^2}{z^2} \sum_{k=1}^{\infty} \frac{\hat{r}_1^2 \theta_k^2 \lambda_k^3 + \frac{1}{n} \hat{r}_2 \lambda_k^2}{(1 + \frac{n}{z} \lambda_k)^2} \\ V = \frac{1}{n\lambda} \sum_{k=1}^d \frac{\lambda_k}{1 + \frac{n}{z} \lambda_k} \end{cases} \quad (55)$$

$$\begin{cases} \hat{r}_1 = \frac{\hat{m}}{V} = \frac{1}{2\pi\sqrt{\rho}} \frac{\sqrt{2\pi} \left[ \operatorname{erf}\left(\frac{1}{\sqrt{2q(1-\eta)}}\right) - \operatorname{erf}\left(\frac{1-V}{\sqrt{2q(1-\eta)}}\right) \right] + 2\sqrt{q(1-\eta)} \left( e^{-\frac{1}{2q(1-\eta)}} - e^{-\frac{(1-V)^2}{2q(1-\eta)}} \right) + \sqrt{2\pi} V \left( 1 + \operatorname{erf}\left(\frac{1-V}{\sqrt{2q(1-\eta)}}\right) \right)}{\int_{\frac{1-V}{\sqrt{q}}}^{\frac{1}{\sqrt{q}}} dx \frac{e^{-\frac{1}{2}x^2}}{\sqrt{2\pi}} \left[1 + \operatorname{erf}\left(\sqrt{\frac{\eta}{2(1-\eta)}}x\right)\right]} \\ \hat{r}_2 = \frac{\frac{\alpha \hat{q}}{V^2}}{\frac{1}{\sqrt{q}} \int_{\frac{1-V}{\sqrt{q}}}^{\frac{1}{\sqrt{q}}} dx \frac{e^{-\frac{1}{2}x^2}}{\sqrt{2\pi}} \left[1 + \operatorname{erf}\left(\sqrt{\frac{\eta}{2(1-\eta)}}x\right)\right] + \frac{1}{\sqrt{q}} \int_{\frac{1-V}{\sqrt{q}}}^{\frac{1}{\sqrt{q}}} dx \frac{e^{-\frac{1}{2}x^2}}{\sqrt{2\pi}} \left[1 + \operatorname{erf}\left(\sqrt{\frac{\eta}{2(1-\eta)}}x\right)\right] (1 - \sqrt{q}x)^2} \left( \int_{\frac{1-V}{\sqrt{q}}}^{\frac{1}{\sqrt{q}}} dx \frac{e^{-\frac{1}{2}x^2}}{\sqrt{2\pi}} \left[1 + \operatorname{erf}\left(\sqrt{\frac{\eta}{2(1-\eta)}}x\right)\right] \right)^2 \end{cases} \quad (56)$$

Specializing to the source/capacity power-law forms (8)

$$\omega_k \sim k^{-\alpha}, \quad \theta_k \sim k^{-\frac{1+\alpha(2r-1)}{2}}, \quad (57)$$

one finally reaches

$$\begin{cases} \rho = \sum_{k=1}^{\infty} k^{-1-2\alpha r} \\ m = \hat{r}_1 \sum_{k=1}^{\infty} \frac{k^{-1-2\alpha r}}{1 + \frac{z}{n} k^\alpha} \\ q = \hat{r}_1^2 \sum_{k=1}^{\infty} \frac{k^{-1-2\alpha r}}{(1 + \frac{z}{n} k^\alpha)^2} + \frac{\hat{r}_2}{n} \sum_{k=1}^{\infty} \frac{1}{(1 + \frac{z}{n} k^\alpha)^2} \\ V = \frac{1}{n\lambda} \frac{z}{n} \sum_{k=1}^{\infty} \frac{1}{1 + \frac{z}{n} k^\alpha} \end{cases} \quad (58)$$

$$\left\{ \begin{aligned} \hat{r}_1 = \frac{\hat{m}}{\hat{V}} &= \frac{1}{2\pi\sqrt{\rho}} \frac{\sqrt{2\pi} \left[ \operatorname{erf}\left(\frac{1}{\sqrt{2q(1-\eta)}}\right) - \operatorname{erf}\left(\frac{1-V}{\sqrt{2q(1-\eta)}}\right) \right] + 2\sqrt{q(1-\eta)} \left( e^{-\frac{1}{2q(1-\eta)}} - e^{-\frac{(1-V)^2}{2q(1-\eta)}} \right) + \sqrt{2\pi}V \left( 1 + \operatorname{erf}\left(\frac{1-V}{\sqrt{2q(1-\eta)}}\right) \right)}{\int_{\frac{1-V}{\sqrt{q}}}^{\frac{1}{\sqrt{q}}} dx \frac{e^{-\frac{1}{2}x^2}}{\sqrt{2\pi}} \left[ 1 + \operatorname{erf}\left(\sqrt{\frac{\eta}{2(1-\eta)}}x\right) \right]} \\ \hat{r}_2 = \frac{\alpha\hat{q}}{\hat{V}^2} &= \frac{V^2 \int_{-\infty}^{\frac{1-V}{\sqrt{q}}} dx \frac{e^{-\frac{1}{2}x^2}}{\sqrt{2\pi}} \left[ 1 + \operatorname{erf}\left(\sqrt{\frac{\eta}{2(1-\eta)}}x\right) \right] + \int_{\frac{1-V}{\sqrt{q}}}^{\frac{1}{\sqrt{q}}} dx \frac{e^{-\frac{1}{2}x^2}}{\sqrt{2\pi}} \left[ 1 + \operatorname{erf}\left(\sqrt{\frac{\eta}{2(1-\eta)}}x\right) \right] (1-\sqrt{q}x)^2}{\left( \int_{\frac{1-V}{\sqrt{q}}}^{\frac{1}{\sqrt{q}}} dx \frac{e^{-\frac{1}{2}x^2}}{\sqrt{2\pi}} \left[ 1 + \operatorname{erf}\left(\sqrt{\frac{\eta}{2(1-\eta)}}x\right) \right] \right)^2} \end{aligned} \right. \quad (59)$$

## B.2. Rate analysis for targets outside the Hilbert space

In the following, we deliver an asymptotic analysis of eqs. (59). To that end, we first ascertain the scaling of the effective regularization  $z$  using the self-consistent equation (54). Depending on the scaling of the order parameter  $V$ , two regimes can be distinguished.

**Effectively regularized regime**  $V \xrightarrow{n \rightarrow \infty} \infty$  In this regime the denominator of (54) scales like

$$\int_{\frac{1-V}{\sqrt{q}}}^{\frac{1}{\sqrt{q}}} dx \frac{e^{-\frac{1}{2}x^2}}{\sqrt{2\pi}} \left[ 1 + \operatorname{erf}\left(\sqrt{\frac{\eta}{2(1-\eta)}}x\right) \right] \approx \frac{1}{\sqrt{q}} \int_{-\infty}^1 dx \frac{e^{-\frac{1}{2}x^2}}{\sqrt{2\pi}} \left[ 1 + \operatorname{erf}\left(\sqrt{\frac{\eta}{2q(1-\eta)}}x\right) \right] = \mathcal{O}\left(\frac{1}{\sqrt{q}}\right), \quad (60)$$

which is exactly the scaling for the corresponding integral in the vanishing regularization case  $\lambda = 0^+$ , see Appendix A eq. (36). In this regime, all the discussion in Appendix A then carries through and the error rate coincides with the one for margin-maximizing SVM (16)

$$\epsilon_g \sim n^{-\frac{\alpha \min(r, \frac{1}{2})}{1 + \alpha \min(r, \frac{1}{2})}}. \quad (61)$$

**Effectively regularized regime**  $V \xrightarrow{n \rightarrow \infty} 0$  The integral in the denominator in (54) then admits the following scaling

$$\int_{\frac{1-V}{\sqrt{q}}}^{\frac{1}{\sqrt{q}}} dx \frac{e^{-\frac{1}{2}x^2}}{\sqrt{2\pi}} \left[ 1 + \operatorname{erf}\left(\sqrt{\frac{\eta}{2(1-\eta)}}x\right) \right] = \frac{1}{\sqrt{q}} \int_{1-V}^1 dx \frac{e^{-\frac{1}{2}x^2}}{\sqrt{2\pi}} \left[ 1 + \operatorname{erf}\left(\sqrt{\frac{\eta}{2q(1-\eta)}}x\right) \right] = \mathcal{O}\left(\frac{V}{\sqrt{q}}\right). \quad (62)$$

This means in particular that

$$z = \frac{Vn\lambda}{\int_{\frac{1-V}{\sqrt{q}}}^{\frac{1}{\sqrt{q}}} dx \frac{e^{-\frac{1}{2}x^2}}{\sqrt{2\pi}} \left[ 1 + \operatorname{erf}\left(\sqrt{\frac{\eta}{2(1-\eta)}}x\right) \right]} = \mathcal{O}(n\lambda\sqrt{q}) \stackrel{\text{def}}{\sim} C_z n^{1-\alpha\gamma}, \quad (63)$$

where we introduced similarly to the max-margin case the to-be determined parameter  $\gamma$ , see also Appendix A. Note that it follows from equation (63) and the definition of  $\lambda = n^{-\ell}$  that

$$q \sim n^{2(\ell-\alpha\gamma)}. \quad (64)$$

Since  $n\lambda V \sim (z/n)^{1-\frac{1}{\alpha}}$ , one also has that

$$V \sim n^{-1+\gamma(1-\alpha)+\ell}. \quad (65)$$

In particular, it can be seen from (65) that the assumption  $V \xrightarrow{n \rightarrow \infty} 0$  only holds for large enough regularizations (slow enough decays  $\ell < \ell^*$  for some limiting value  $\ell^*$ ), satisfying

$$-1 + \gamma(1 - \alpha) + \ell < 0. \quad (66)$$



The regularization decay  $\ell = \ell^*$  gives the boundary between the effectively regularized and unregularized regime. Because of this, the rate of  $q$  at  $\ell^*$  should coincide with its max-margin rate (15). This, together with (66), allow to determine  $\ell^*$  as the solution of the system (denoting  $\gamma^*$  the value of  $\gamma$  at  $\ell = \ell^*$ )

$$\begin{cases} -1 + \gamma^*(1 - \alpha) + \ell = 0, \\ \ell^* - \alpha\gamma^* = \frac{\alpha \min(r, \frac{1}{2})}{1 + \alpha \min(r, \frac{1}{2})}, \end{cases} \quad (67)$$

viz.

$$\ell^* = \alpha \frac{1 + \min(r, \frac{1}{2})}{1 + \alpha \min(r, \frac{1}{2})}. \quad (68)$$

Summarizing, for  $\ell > \ell^*$ , in the effectively unregularized regime, the max-margin scalings (15), (16) hold. In the following, we focus on pursuing the discussion for the new  $\ell < \ell^*$  (effectively regularized) regime.

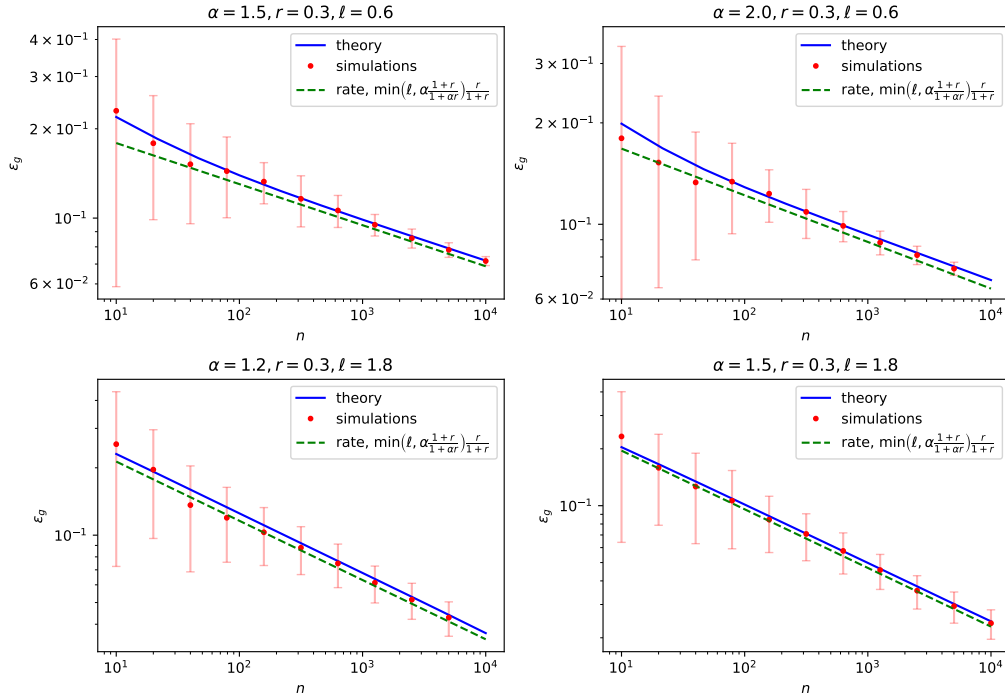


Figure 6. Misclassification error  $\epsilon_g$  for hinge classification on synthetic Gaussian data, as specified in (8), for different source/capacity coefficients  $\alpha, r$ , for a regularization  $\lambda = n^{-\ell}$ . In blue, the solution of the closed set of equations (53) used in the characterization (9) for the misclassification error, using the `g3m` package (Loureiro et al., 2021). The dimension  $p$  was cut-off at  $10^4$ . Red dots corresponds to simulations using the `scikit-learn` SVC package and averaged over 40 instances, for  $p = 10^4$ . The green dashed line indicates the power-law rate (73) derived in this work.

The expansion for  $m$  and  $q$  carry over in similar fashion to max-margin (see Appendix A), yielding

$$\begin{cases} m = \hat{r}_1 \left[ \rho - \mathbb{1}_{r \geq \frac{1}{2}} C_z A_m^n n^{-\gamma\alpha} - C_z n^{-2\gamma\alpha} \int_{\Theta(r-\frac{1}{2})}^{\infty} \frac{x^{-1+\alpha(1-2r)}}{1+C_z x^\alpha} \right] + o\left(\max(n^{-\gamma\alpha}, n^{-2\gamma\alpha})\right), \\ q = \hat{r}_1^2 \left[ \rho + \frac{\hat{r}_2}{\hat{r}_1^2} n^{\gamma-1} \int_0^{\infty} \frac{1}{(1+C_z x^\alpha)^2} - \mathbb{1}_{r \geq \frac{1}{2}} 2C_z A_q^n n^{-\gamma\alpha} - \mathbb{1}_{r \geq 1} C_z^2 B_q^n n^{-2\gamma\alpha} \right. \\ \left. - n^{-2\gamma\alpha} \left( 2C_z \int_{\Theta(r-\frac{1}{2})}^{\infty} \frac{x^{-1+\alpha(1-2r)}}{(1+C_z x^\alpha)^2} + C_z^2 \int_{\Theta(r-1)}^{\infty} \frac{x^{-1+\alpha(2-2r)}}{(1+C_z x^\alpha)^2} \right) \right] + o\left(\max\left(\frac{\hat{r}_2}{\hat{r}_1^2} n^{\gamma-1}, n^{-\gamma\alpha}, n^{-2\gamma\alpha}\right)\right). \end{cases}$$

Therefore  $\hat{r}_1 \sim \sqrt{q} \sim n^{\ell-\alpha\gamma}$ , while a rescaling of the integrals in the equations for  $\hat{r}_2$  also reveal that  $\hat{r}_2 \sim \hat{r}_1 \sim \sqrt{q} \sim n^{\ell-\alpha\gamma}$ . Summarizing

$$m \sim \hat{r}_2 \sim \hat{r}_1 \sim \sqrt{q} \sim n^{\ell-\alpha\gamma}. \quad (69)$$

Note that the mutual scaling of the order parameters  $m, q, \hat{r}_1$  is the same as for max-margin classification (15), which is the mutual scaling directly following from the physical interpretation of  $m, q$  as  $\langle \hat{w}, \theta^* \rangle_{L^2(\mathcal{X})}$ ,  $\|\hat{w}\|_{L^2(\mathcal{X})}^2$  and of  $\hat{r}_1$  as  $\|\hat{w}\|_{L^2(\mathcal{X})}^2 / \|\theta^*\|_{L^2(\mathcal{X})}^2$ , see also discussion in section 2 under equation (12). Finally,

$$\begin{aligned} \eta &= \frac{\left(1 - \mathbb{1}_{r \geq \frac{1}{2}} C_z \frac{A_m^n}{\rho} n^{-\gamma\alpha} - n^{-2\gamma\alpha r} \frac{C_z}{\rho} \int_{\Theta(r-\frac{1}{2})}^{\infty} \frac{x^{-1+\alpha(1-2r)}}{1+C_z x^\alpha} \right)^2}{1 + \frac{\hat{r}_2}{\rho \hat{r}_1^2} n^{\gamma-1} \int_0^{\infty} \frac{1}{(1+x^\alpha)^2} - \frac{\mathbb{1}_{r \geq \frac{1}{2}} 2C_z A_q^n n^{-\gamma\alpha} - \mathbb{1}_{r \geq 1} C_z^2 B_q^n n^{-2\gamma\alpha}}{\rho} - n^{-2\gamma\alpha r} \frac{C_z}{\rho} \left( 2 \int_{\Theta(r-\frac{1}{2})}^{\infty} \frac{x^{-1+\alpha(1-2r)}}{(1+C_z x^\alpha)^2} + C_z \int_{\Theta(r-1)}^{\infty} \frac{x^{-1+\alpha(2-2r)}}{(1+C_z x^\alpha)^2} \right)} \\ &= 1 - \mathcal{O}\left(\frac{\hat{r}_2}{\rho \hat{r}_1^2} n^{\gamma-1}\right) + \mathbb{1}_{r \geq 1} \mathcal{O}(n^{-2\gamma\alpha}) + \mathcal{O}(n^{-2\gamma\alpha r}) \\ &= 1 - \mathcal{O}\left(n^{\gamma(\alpha+1)-1-\ell}\right) + \mathcal{O}(n^{-2\alpha\gamma r}), \end{aligned} \quad (70)$$

where we specialized to  $r \leq \frac{1}{2}$  in the last line, thereby focusing on target functions  $f^* \in L^2(\mathcal{X}) \setminus \mathcal{H}$ . At this point, it remains to heuristically determine  $\gamma$ , a rigorous analytical derivation of our results being left for future work. Making the two (numerically verified) assumptions

**Assumption B.1.** Like the max-margin case,  $1 - \eta \sim q^{-1}$ ,

**Assumption B.2.** The term of rate  $2\alpha\gamma r$  dominates in (70).

$\gamma$  can be guessed as

$$\gamma = \frac{\ell}{\alpha(1+r)}. \quad (71)$$

Note that consistently, the value of  $\gamma$  at the boundary  $\ell = \ell^*$  with the unregularized regime  $\gamma^*$  coincides with its max-margin value (51). In the effectively regularized regime, under these assumptions, we thus conjecture the error to scale for  $r \leq \frac{1}{2}$  as

$$\epsilon_g \sim \sqrt{1-\eta} \sim n^{\alpha\gamma-\ell} \sim n^{-\ell \frac{r}{1+r}}. \quad (72)$$

Finally observe that the rates for the effectively unregularized regime  $\ell \geq \ell^*$  (61) and regularized regime  $\ell \leq \ell^*$  (72) can be subsumed in the more compact form, still for  $r \leq \frac{1}{2}$ :

$$\epsilon_g \sim n^{-\min(\ell, \ell^*) \frac{r}{1+r}} = n^{-\min(\ell, \alpha \frac{1+r}{1+\alpha r}) \frac{r}{1+r}}. \quad (73)$$

Fig. 6 contrasts the rates (73) to the numerical solution of the equations (53) and to numerical simulations, and displays a very good agreement. The main conclusion from (73) is that for any  $\ell$ , the rate is *necessarily slower* than  $\ell^* r / (1+r) = \alpha r / (1+\alpha r)$ , which is the max-margin rate (16). Therefore, the max-margin rate (16) is optimal for  $r \leq \frac{1}{2}$ , and is achieved for any regularization  $\lambda$  decaying at least as fast as  $n^{-\ell^*}$ . In particular, it is achieved for the limit case  $\ell = \infty$ , i.e.  $\lambda = 0^+$  a.k.a. the max-margin case, thereby suggesting that no regularization is optimal for rough enough target functions  $f^* \in L^2(\mathcal{X}) \setminus \mathcal{H}$ . Since regularization is not needed for hard teachers (small source  $r$ ), we do not a fortiori expect it to help for easier, smoother teachers  $f^* \in \mathcal{H}$  characterized by source  $r \geq \frac{1}{2}$ . This suggests that  $\lambda = 0^+$  (max-margin) should be optimal for all sources  $r$ , i.e. any target  $f^* \in L^2(\mathcal{X})$ . While this conjecture is observed to hold in numerical simulations, a more thorough theoretical analysis of the error rates for  $r \geq \frac{1}{2}$  is nevertheless warranted. We leave this more challenging analysis to future work.

### C. Rates for ridge classification

In this section we derive the rates (21) for ridge classifiers.

### C.1. Ridge classification under the source and capacity conditions

The equations on  $m$ ,  $q$  for ridge classification (Loureiro et al., 2021) can as in Appendix A be adapted to the  $p = \infty$ ,  $n \gg 1$  limit as

$$\begin{cases} m = \hat{m}p \frac{\text{tr} \frac{\Sigma \theta^* \theta^{*\top} \Sigma}{n\lambda + p\hat{V}\Sigma}}{n\lambda + p\hat{V}\Sigma} \\ q = p \text{tr} \frac{p\hat{m}^2 \Sigma \theta^* \theta^{*\top} \Sigma^2 + \hat{q}\Sigma^2}{(n\lambda + p\hat{V}\Sigma)^2} \\ V = \text{tr} \frac{\Sigma}{n\lambda + p\hat{V}\Sigma} \end{cases}, \quad \begin{cases} \hat{V} = \frac{\frac{n}{p}}{1+V} \\ \hat{q} = \frac{n}{p} \frac{1+q-2m\sqrt{\frac{2}{\pi\rho}}}{(1+V)^2} = \frac{\hat{V}^2}{\frac{n}{p}} \left(1 + q - 2m\sqrt{\frac{2}{\pi\rho}}\right) \\ \hat{m} = \sqrt{\frac{2}{\pi\rho} \frac{\frac{n}{p}}{1+V}} = \sqrt{\frac{2}{\pi\rho} \hat{V}}. \end{cases} \quad (74)$$

Following (Cui et al., 2021), we introduce the effective regularization  $z$

$$z = \frac{\frac{n}{p}n\lambda}{\hat{V}} = n\lambda + \frac{z}{n} \sum_{k=1}^{\infty} \frac{\lambda_k}{\lambda_k + \frac{z}{n}} \approx n\lambda + \left(\frac{z}{n}\right)^{1-\frac{1}{\alpha}} \int_{\left(\frac{z}{n}\right)^{\frac{1}{\alpha}}}^{\infty} \frac{dx}{1+x^{\alpha}}. \quad (75)$$

Like in Appendix A, we denote  $z \sim C_z n^{1-\alpha\gamma}$  the scaling of  $z$ . In contrast to Appendices A and B for SVM, the exponent  $\gamma$  for ridge classifier can be straightforwardly determined. Depending on the relative strength of the two terms in (75), two possible values for  $\gamma$  exist:

- $\gamma = \frac{\ell}{\alpha}$  if  $n\lambda \gg (z/n)^{1-1/\alpha}$  in (75), i.e.  $\ell < \alpha$ . This correspond to the *effectively regularized regime* (Cui et al., 2021).
- $\gamma = 1$  if  $n\lambda \ll (z/n)^{1-1/\alpha}$  in (75), i.e.  $\ell > \alpha$ . In this regime, the regularization  $\lambda$  is negligible and therefore the learning is *effectively un-regularized* (Cui et al., 2021).

Rewriting the equations (74) using (75), the equations (18) of the main text are reached (see section 4):

$$\begin{cases} \rho = \sum_{k=1}^{\infty} k^{-1-2\alpha r} \\ m = \sqrt{\frac{2}{\pi\rho}} \sum_{k=1}^{\infty} \frac{k^{-1-2\alpha r}}{1+\frac{z}{n}k^{\alpha}} \\ q = \frac{2}{\pi\rho} \sum_{k=1}^{\infty} \frac{k^{-1-2\alpha r}}{(1+\frac{z}{n}k^{\alpha})^2} + \frac{1+q-2m\sqrt{\frac{2}{\pi\rho}}}{n} \sum_{k=1}^{\infty} \frac{1}{(1+\frac{z}{n}k^{\alpha})^2} \\ V = \frac{z}{n^2\lambda} \sum_{k=1}^{\infty} \frac{1}{1+\frac{z}{n}k^{\alpha}} \end{cases}. \quad (76)$$

### C.2. Scaling analysis

We proceed to deliver an scaling analysis of eqs. (18). We know from Appendix A the following scalings

$$\begin{cases} m = \sqrt{\frac{2}{\pi\rho}} \left[ \rho - \mathbb{1}_{r \geq \frac{1}{2}} C_z A_m^n n^{-\gamma\alpha} - n^{-2\gamma\alpha r} C_z \int_{\Theta(r-\frac{1}{2})}^{\infty} \frac{x^{-1+\alpha(1-2r)}}{1+C_z x^{\alpha}} \right] + o(\max(n^{-\gamma\alpha}, n^{-2\gamma\alpha r})), \\ q = \frac{2}{\pi\rho} \left[ \rho + \frac{\pi\rho C_z}{2} \left(1 + q - 2m\sqrt{\frac{2}{\pi\rho}}\right) n^{\gamma-1} \int_0^{\infty} \frac{1}{(1+C_z x^{\alpha})^2} - \mathbb{1}_{r \geq \frac{1}{2}} 2C_z A_q^n n^{-\gamma\alpha} - \mathbb{1}_{r \geq 1} C_z^2 B_q^n n^{-2\gamma\alpha} \right. \\ \left. - n^{-2\gamma\alpha r} \left( 2C_z \int_{\Theta(r-\frac{1}{2})}^{\infty} \frac{x^{-1+\alpha(1-2r)}}{(1+C_z x^{\alpha})^2} + C_z^2 \int_{\Theta(r-1)}^{\infty} \frac{x^{-1+\alpha(2-2r)}}{(1+C_z x^{\alpha})^2} \right) \right] + o\left(\max\left(\frac{\hat{r}_2}{\hat{r}_1^2} n^{\gamma-1}, n^{-\gamma\alpha}, n^{-2\gamma\alpha r}\right)\right). \end{cases}$$

Once again, we defined the shorthands

$$A_m^n \stackrel{\text{def}}{=} \sum_{k=1}^{n^{\gamma}} \frac{k^{-1-2\alpha(r-\frac{1}{2})}}{1+C_z \left(\frac{k}{n^{\gamma}}\right)^{\alpha}}, \quad A_q^n \stackrel{\text{def}}{=} \sum_{k=1}^{n^{\gamma}} \frac{k^{-1-2\alpha(r-\frac{1}{2})}}{\left(1+C_z \left(\frac{k}{n^{\gamma}}\right)^{\alpha}\right)^2}, \quad B_q^n \stackrel{\text{def}}{=} \sum_{k=1}^{n^{\gamma}} \frac{k^{-1-2\alpha(r-1)}}{\left(1+C_z \left(\frac{k}{n^{\gamma}}\right)^{\alpha}\right)^2}. \quad (77)$$

We remind that, similarly to the discussion in Appendix A, the sequences  $A_m^n$  and  $A_q^n$  admit identical limits as  $n \rightarrow \infty$ :  $A_q^\infty = A_m^\infty$ . The consequences of this identity are expounded below. We now focus on ascertaining the scalings of the order parameters  $m$ ,  $q$ . These scalings depend on the regime considered.

**Regularized regime  $\ell < \alpha$**  In the case  $\ell < \alpha$ , we have  $\gamma = \ell/\alpha < 1$ . Then the expansion for  $q$  reads

$$q(1 - o(1)) = \frac{2}{\pi\rho} \left( \rho - \mathbb{1}_{r \geq \frac{1}{2}} 2C_z A_q^n n^{-\ell} \right) - \mathcal{O} \left( n^{-2\ell \min(r,1)} \right) - \frac{4-\pi}{\pi} C_z n^{-\frac{\alpha-\ell}{\alpha}} \int_0^\infty \frac{1}{(1+C_z x^\alpha)^2}, \quad (78)$$

from which it follows that

$$q = \frac{2}{\pi\rho} \left( \rho - \mathbb{1}_{r \geq \frac{1}{2}} 2A_q^n n^{-\ell} \right) - \mathcal{O} \left( n^{-\min(2\ell \min(r,1), \frac{\alpha-\ell}{\alpha})} \right). \quad (79)$$

Therefore the cosine similarity  $\eta$  admits the following expression

$$\eta = \frac{m^2}{\rho q} = \frac{\frac{2}{\pi\rho} \rho^2 \left[ 1 - \mathbb{1}_{r \geq \frac{1}{2}} \frac{A_m^n}{\rho} n^{-\ell} + \mathcal{O} \left( n^{-2\ell r} \right) \right]^2}{\frac{2}{\pi\rho} \rho^2 \left[ 1 - \mathbb{1}_{r \geq \frac{1}{2}} \frac{2A_q^n}{\rho} n^{-\ell} - \mathcal{O} \left( n^{-\min(2\ell \min(r,1), \frac{\alpha-\ell}{\alpha})} \right) \right]} = 1 - \mathcal{O} \left( n^{-\min(2\ell \min(r,1), \frac{\alpha-\ell}{\alpha})} \right), \quad (80)$$

where we used that  $A_q^n$  and  $A_m^n$  share the same limit. Finally, the scaling for the misclassification error can be accessed:

$$\epsilon_g \sim \sqrt{1-\eta} \sim n^{-\frac{1}{2} \min(2\ell \min(r,1), \frac{\alpha-\ell}{\alpha})}, \quad (81)$$

which is equation (21).

*Remark C.1.* Note that only the classification error (9) tends to zero, while neither the MSE between the label  $y = \text{sign}(\theta^{\star\top} \psi(x))$  and the pre-activation linear predictor  $\hat{w}^\top \psi(x)$  (below denoted  $\text{MSE}_1$ ) nor the MSE between the teacher and student preactivations  $\theta^{\star\top} \psi(x)$ ,  $\hat{w}^\top \psi(x)$  (below denoted  $\text{MSE}_2$ ) tend to zero.

$$\text{MSE}_1 = \mathbb{E}_{\psi(x)} \left( \text{sign}(\theta^{\star\top} \psi(x)) - \hat{w}^\top \psi(x) \right)^2 = 1 + q - 2m \sqrt{\frac{2}{\pi\rho}} \xrightarrow{n \rightarrow \infty} 1 - \frac{2}{\pi} \quad (82)$$

$$\text{MSE}_2 = \mathbb{E}_{\psi(x)} \left( \theta^{\star\top} \psi(x) - \hat{w}^\top \psi(x) \right)^2 = \rho + q - 2m \xrightarrow{n \rightarrow \infty} \rho \left( 1 - \sqrt{\frac{2}{\pi\rho}} \right)^2 \quad (83)$$

Note also the identity between the order parameter  $\hat{r}_2$  and  $\text{MSE}_1$ :  $\hat{r}_2 = \text{MSE}_1$ , discussed in section 4 in the main text.

**Unregularized regime  $\ell > \alpha$**  If  $\ell > \alpha$ , then  $\gamma = 1$  and

$$q \left( 1 - C_z \int_0^\infty \frac{1}{(1+C_z x^\alpha)^2} \right) = \frac{2}{\pi} - \frac{4-\pi}{\pi} C_z \int_0^\infty \frac{1}{(1+C_z x^\alpha)^2} - \mathcal{O} \left( n^{-2\alpha \min(r, \frac{1}{2})} \right) \quad (84)$$

Hence

$$\eta = \frac{m^2}{\rho q} \xrightarrow{n \rightarrow \infty} \frac{1 - C_z \int_0^\infty \frac{1}{(1+C_z x^\alpha)^2}}{1 - \frac{4-\pi}{2} C_z \int_0^\infty \frac{1}{(1+C_z x^\alpha)^2}} \neq 1. \quad (85)$$

Since  $\eta$  is now bounded away from 1, the misclassification error  $\epsilon_g$  fails to go to 0 asymptotically, and plateaus to a finite value:

$$\epsilon_g = \mathcal{O}(1), \quad (86)$$

which is equation (22). This plateau is attributable to ridge classifiers overfitting the binary labels, see Appendix D for further discussion.

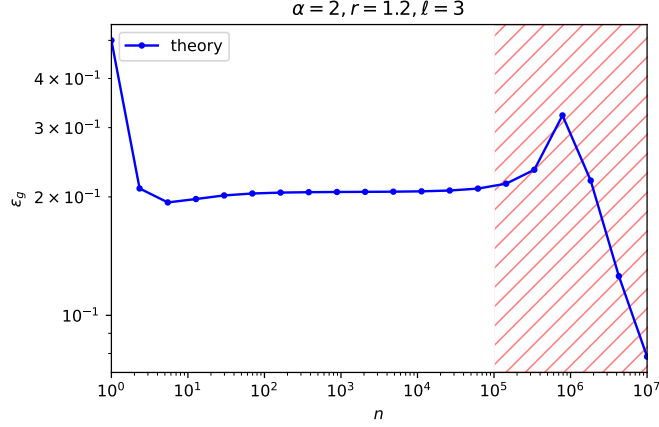


Figure 7. Misclassification error  $\epsilon_g$  for ridge classification on artificial Gaussian data, as specified in (8), for source  $r = 1.2$ , capacity  $\alpha = 2$ , at regularization  $\lambda = n^{-3}$ . The dimension was cut-off to  $p = 10^6$ . The blue curve corresponds to the numerical solution of the equations (18) using the `g3m` package (Loureiro et al., 2021). While for sample complexities comparable or larger than the dimension  $n \geq p$  a second descent, followed by a drop of the error to zero, is observable, in the  $1 \ll n \ll p = \infty$  limit considered in the present work the second descent, which happens for  $n \gtrsim p$  (red hashed region), is no longer observed. Instead, only the plateau following the first descent is observed, which corresponds to the saturation effect of Fig. 3

## D. Remark on the overfitting regime of ridge classification

In this Appendix, we provide further discussion on the saturation of the error (9) to a finite value in the effectively unregularized regime of ridge classification (22), which defies the common intuition that for large enough sample complexity  $n$ , ridge classification should be able to generalize almost perfectly. In this section, we first provide an analytical reminder of why the error does go to zero for finite-dimensional feature spaces ( $p < \infty$ ,  $n \gg 1$ ), before discussing what differs in the setup at hand ( $1 \ll n \ll p = \infty$ ). We argue that while in the first limit a double-descent phenomenon is observed, the second limit always corresponds to a learning regime located in the plateau/valley following the first descent. In the following, we consider directly the  $\lambda = 0$  case for the sake of simplicity.

### D.1. The finite dimensional setup

We first sketch up an brief analysis for the limit of finite feature space dimension  $\infty > p \gg 1$  setting, with large sample complexity  $n \gg p$ . Naming  $X \in \mathbb{R}^{n \times p}$  (with the  $\mu^{\text{th}}$  row of  $X$  being  $\psi(x^\mu)$ ) the matrix of the data in feature space and  $y = \text{sign}(X\theta^*) \in \mathbb{R}^n$  the corresponding vector of stacked labels, the ridge estimator can be compactly written as

$$\hat{w} = (X^T X)^{-1} X^T \text{sign}(X\theta^*). \quad (87)$$

In the  $n \rightarrow \infty$  limit

$$\frac{1}{n} X^T X = \Sigma + \mathcal{O}\left(\frac{1}{\sqrt{n}}\right), \quad \frac{1}{n} X^T \text{sign}(X\theta^*) = \mathbb{E}_x^{\mathcal{N}(0, \Sigma)} [x \text{sign}(x \cdot \theta^*)] + \mathcal{O}\left(\frac{1}{\sqrt{n}}\right). \quad (88)$$

Hence

$$\begin{aligned} \hat{w} &\approx \Sigma^{-1} \mathbb{E}_x^{\mathcal{N}(0, \Sigma)} [x \text{sign}(\theta^{*T} x)] \\ &\approx \Sigma^{-1} \Sigma^{\frac{1}{2}} \mathbb{E}_x^{\mathcal{N}(0, \mathbb{1})} [x \text{sign}(x^T \Sigma^{\frac{1}{2}} \theta^*)] \\ &\approx \Sigma^{-\frac{1}{2}} \mathbb{E}_{x_{\parallel}}^{\mathcal{N}(0, \mathbb{1})} [x_{\parallel} \text{sign}(x_{\parallel})] \frac{\Sigma^{\frac{1}{2}} \theta^*}{\|\Sigma^{\frac{1}{2}} \theta^*\|_2}. \end{aligned} \quad (89)$$

So

$$\hat{w} = \sqrt{\frac{2}{\pi}} \frac{\theta^*}{\|\Sigma^{\frac{1}{2}} \theta^*\|_2} \propto \theta^*. \quad (90)$$



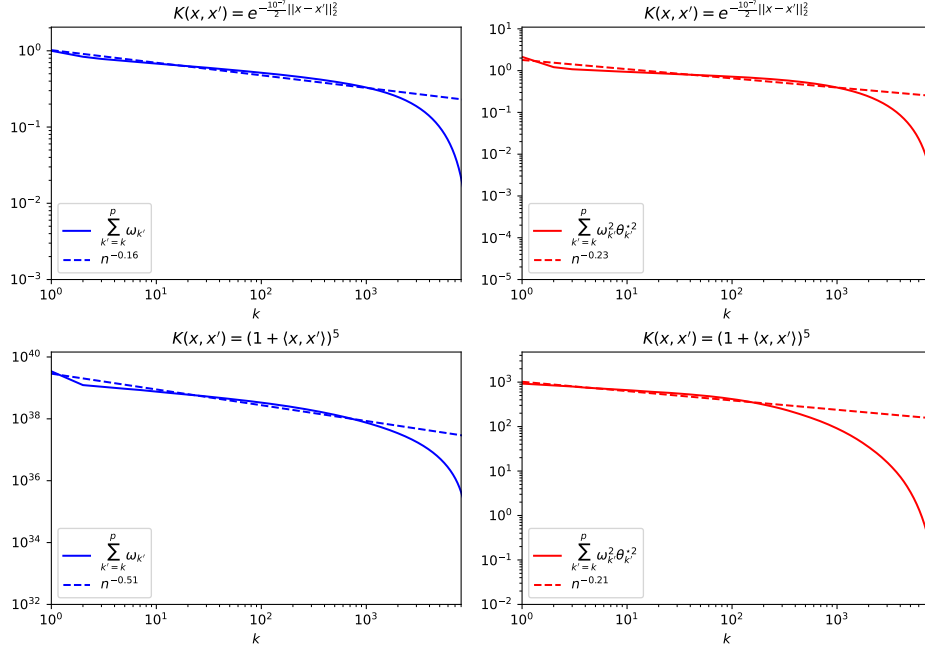


Figure 8. Cumulative functions (94) for  $10^4$  CIFAR 10 sampled at random, for a RBF kernel (top) and a polynomial kernel (bottom). The slopes fitted using least-squares linear regression on the regions the curves are qualitatively resembling power-laws are represented in dashed lines.

This means in particular the direction of the teacher is perfectly recovered, and that the prediction error  $\epsilon_g$  (9) goes to zero in the  $p \ll n \rightarrow \infty$  limit.

## D.2. Infinite dimensional feature space

We now argue why this discussion ceases to hold in the setup of interest  $n \ll p = \infty$  (plateau reached after the first descent, see Fig. 7). In this limit, loosely written,

$$\begin{aligned} \hat{w} &\approx \left( \Sigma^{-1} + \mathcal{O}\left(\frac{1}{\sqrt{n}}\right) \right) \left( \mathbb{E}_x^{\mathcal{N}(0, \Sigma)} [x \text{sign}(\theta^{*T} x)] + \mathcal{O}\left(\frac{1}{\sqrt{n}}\right) \right) \\ &= \sqrt{\frac{2}{\pi}} \frac{\theta^*}{\|\Sigma^{\frac{1}{2}} \theta^*\|_2} + \mathcal{O}\left(\sqrt{\frac{p}{n}}\right) \neq \text{cte.} \times \theta^*. \end{aligned} \quad (91)$$

The last term comes from the sum of  $p$  random terms of order  $1/\sqrt{n}$  entailed by the matrix multiplication. In particular, this implies that the teacher fails to be perfectly recovered by ERM in this limit, causing the misclassification error to plateau to a finite limit, see equation (22). This is due to the fact that in an infinite-dimensional space, the ridge ERM (17) always has enough dimensions to overfit the dataset. Another way to look at this limit is in the framework of the well-known *double-descent* phenomenon which occurs in the finite dimensional limit  $p < \infty$  discussed in subsection D.1. In the  $p = \infty$  limit, the second descent, which commences at  $n \approx p$ , happens at infinite sample complexity and is thus not observed for finitely large  $n$ . In fact, the  $1 \ll n \ll p = \infty$  limit always correspond to the plateau following the first descent, see Fig. 7.

## E. Details on real datasets

### E.1. Measuring the capacity and source of real datasets

In this section we provide details on the experiments on real data (section 5, Fig. 5), which can also be found in (Spigler et al., 2020; Bordelon et al., 2020; Cui et al., 2021). Consider a real dataset  $\mathcal{D}_m = \{x^\mu, y^\mu\}_{\mu=1}^m$  of size  $m$ . The data distribution  $\nu$

defined in section 2 is then the empirical distribution over  $\mathcal{D}_m$ :

$$\nu(\cdot) = \frac{1}{n} \sum_{\mu=1}^m \delta(\cdot - x^\mu). \quad (92)$$

Then the definitions of the feature map  $\psi$  (3) and of the feature covariance  $\Sigma$  (5) admit the simple rewriting

$$\frac{1}{m} G \Psi = \Psi \Sigma, \quad \Sigma = \frac{1}{m} \Psi^\top \Psi, \quad (93)$$

provided we introduce the Gram matrix  $G_{\mu,\nu} = K(x^\mu, x^\nu) \in \mathbb{R}^{m \times m}$  and the matrix of horizontally stacked features  $\Psi_{\mu k} = \psi(x^\mu)_k \in \mathbb{R}^{m \times m}$ . Note that for real data, one has that the dimension of the feature space  $p$  is equal to the total size of the dataset  $m$ . A teacher  $\theta^*$  providing perfect classification  $y = \text{sign}(\Psi \theta^*)$  can be found e.g. by performing max margin classification on  $(\Psi, y)$ . While the method to fit a perfect classifier  $\theta^*$  is not unique, we observed that using logistic classifiers or regularized hinge classifiers instead of max-margin classifiers did not significantly impact the measured source coefficient.

From the eigenvalues  $\{\omega_k\}_{k=1}^p$  of the covariance  $\Sigma$  (93) and the components of the teacher  $\{\theta_k^*\}_{k=1}^p$ , the capacity and source  $\alpha, r$  (8) can be estimated. From (8), the following scalings should hold:

$$\sum_{k'=k}^p \omega_{k'} \sim k^{1-\alpha}, \quad \sum_{k'=k}^p \omega_{k'} \theta_{k'}^{*2} \sim k^{-2\alpha r}. \quad (94)$$

These curves are presented in Fig. 8 for the dataset comprised of  $10^4$  randomly samples CIFAR 10 images, see section 5 of the main text. Note that we estimate the cumulative functions (94) following (Spigler et al., 2020; Cui et al., 2021) because the summation allows to smoothen out the curves, thus permitting a relatively more precise evaluation. Because the feature space is finite, the functions (94) fail to be exact power-laws, and exhibit in particular a sharp drop for  $n$  approaching  $m$ . Nonetheless, we identify for each curve a region of indices  $k$  for which the curve looks qualitatively like a power-law, and fit the curves by a power-law using least-squares linear regression to finally extract the coefficients  $\alpha, r$  therefrom. These fits are shown in Fig. 8 for the reduced CIFAR 10 dataset discussed in the main text (see section 5), for an RBF kernel with inverse variance  $10^{-7}$  and a polynomial kernel of degree 5. The capacity and source were estimated to be  $\alpha \approx 1.16$ ,  $r \approx 0.10$  for the RBF kernel and  $\alpha \approx 1.51$ ,  $r \approx 0.07$  for the polynomial kernel.

## E.2. Details on numerical simulations

In this subsection, we provide further details on the simulations presented in Fig. 5 of the main text. For each sample complexity  $n$ , a subset of size  $n$  was randomly sampled without replacements from  $\mathcal{D}_m$ . Like in (Canatar et al., 2021; Loureiro et al., 2021; Cui et al., 2021), the whole dataset  $\mathcal{D}_m$  was used as a test set. The max-margin simulations in Fig. 5 were performed using the `scikit-learn` `SVC` package at vanishing regularization  $\lambda = 10^{-5}$ , and averaged over 50 realizations of the training set. The ridge simulations in Fig. 5 were realized using the `scikit-learn` `KernelRidge` package, with the optimal  $\lambda$  estimated using `scikit-learn` `GridSearchCV`'s default 5-fold cross validation routine over a grid  $\lambda \in \{0\} \cup (10^{-10}, 10^5)$ , with logarithmic step size  $\delta \log \lambda = 0.026$ . The misclassification error was also averaged over 50 realizations of the training set.